

A scalable multidimensional fully implicit solver for Hall magnetohydrodynamics

L. Chacón^{a,*}

^a*Los Alamos National Laboratory, Los Alamos, NM 87545, USA*

Abstract

We propose an optimally performant fully implicit algorithm for the Hall magnetohydrodynamics (HMHD) equations based on multigrid-preconditioned Jacobian-free Newton-Krylov methods. HMHD is a challenging system to solve numerically because it supports stiff fast dispersive waves. The preconditioner is formulated using an operator-split approximate block factorization (Schur complement), informed by physics insight. We use a vector-potential formulation (instead of a magnetic field one) allow a clean segregation of the problematic $\nabla \times \nabla \times$ operator in the electron Ohm's law subsystem. This segregation allows the formulation of an effective damped block-Jacobi smoother for multigrid. We demonstrate by analysis that our proposed block-Jacobi iteration is convergent and has the smoothing property. The resulting HMHD solver is verified linearly with wave propagation examples, and nonlinearly with the GEM challenge reconnection problem by comparison against another HMHD code. We demonstrate the excellent algorithmic and parallel performance of the algorithm up to 16384 MPI tasks in two dimensions.

Keywords: implicit methods, Hall magnetohydrodynamics, Newton-Krylov, multigrid, physics-based preconditioning, approximate block factorization.

1. Introduction

We propose a scalable implicit algorithm for the Hall magnetohydrodynamics (HMHD) model, which is of relevance in the modeling of astrophysical, magnetospheric, and laboratory (e.g., fusion) plasmas. HMHD is well known to support fast dispersive waves, which become very stiff numerically with increasing spatial resolution, resulting in explicit Courant-Friedrichs-Lewy (CFL) timestep stability constraints scaling quadratically with the mesh spacing rather than linearly. As a result, the explicit integration of this system becomes very expensive for sufficiently refined meshes, encouraging the exploration of implicit methods.

Several authors have attempted to build implicitness in the solution algorithm of the HMHD equations over the years. The earliest study we are aware of is Ref. [1], where a semi-implicit solver for the HMHD system based on a pseudospectral discretization in cylindrical geometry was proposed for out-of-plane uniform magnetic fields (which incidentally do not propagate the problematic stiff hyperbolic waves mentioned earlier). The stability analysis of the semi-implicit time-advance formulation in the general case (including stiff hyperbolic waves) was studied in Ref. [2], concluding that strict time-centering was needed for numerical stability. Several authors have explored fully implicit HMHD formulations, either in its reduced form (i.e., assuming plasma incompressibility) [3, 4, 5, 6, 7] or in primitive-variable form [5, 8, 9, 10, 11, 12]. Of these, many of them employ either direct solvers [4, 5, 6, 11, 12] or incomplete LU factorizations [10], which are known not to scale well either algorithmically under grid refinement, or in parallel (and in fact little information is provided about either scaling in the references). Scalable fully implicit solutions for the

*Corresponding author

Email address: chacon@lanl.gov (L. Chacón)

reduced HMHD system [3, 7] and the primitive-variable HMHD system in a non-standard ion formulation [8] were proposed that show significant promise. However, the latter formulation (relevant to the present study) has been found by the author to be prone to numerical noise from fast dispersive waves, and problematic to solve when attempting to include high-order dissipation (via hyperresistivity, mimicking electron viscosity [13]) to control it. Other authors have attempted to bypass the numerical stiffness challenges of HMHD either by adding a fictitious displacement current term in Ampere’s law [14, 15] or by reverting back to a multi-fluid formulation with promising approximate block-factorization preconditioners [16, 17]. The former approach is problematic because the formulation is physically inconsistent, and can be shown to introduce instability [15]. The latter introduces a large number of additional equations, and features fast charge-separation and lightwave timescales that complicate an implicit treatment (although these could be important in some physical contexts such as the treatment of boundary sheaths).

This paper builds on earlier work [18] where a scalable, parallel, fully implicit, fully nonlinear solver for the 3D resistive compressible MHD equations was demonstrated, and augments it to include electron Hall and pressure effects. As in the reference, we base our nonlinear solver approach on the Newton-Raphson iterative algorithm. Krylov iterative techniques [19], implemented Jacobian-free [20, 21] (i.e., without ever forming and storing the Jacobian matrix) for memory efficiency, are employed for the required algebraic matrix inversions. Here, FGMRES (Flexible Generalized Minimal RESiduals [22, 23]) is employed as the Krylov solver of choice, due to the lack of symmetry in the algebraic system of interest. The flexible character of FGMRES allows the preconditioner to change between successive GMRES iterations. We will exploit this feature in our implementation.

The efficiency and scalability of Krylov methods depends strongly on adequate preconditioning [19]. In Refs. [3, 18], a suitable multigrid-based preconditioner is developed for the MHD system around the parabolization concept, whereby a hyperbolic system is reformulated as a parabolic one using a Schur factorization, which is in turn amenable to a multilevel treatment. The parabolization procedure is generalized here to HMHD. Using physics insight, we approximate the exact Schur factorization with an operator-split procedure, where the stiff electron subsystem (which we will term electron MHD, or EMHD) is inverted first, followed by the ion MHD subsystem inversion proposed in Ref. [18]. All subsystems are solved using a fully parallel geometric multigrid (MG) implementation based on a coarse-grid parallel-domain agglomeration strategy (similar to that proposed in Refs. [24, 25]). For the EMHD subsystem (which is the stiffest one in HMHD), we propose a novel six-equation block damped-Jacobi smoothing strategy that is shown by analysis to lead to convergent Jacobi iterations and to possess the smoothing property. Damped Jacobi is demonstrated in Ref. [9] to be a viable smoother for a semi-implicit discretization of the 2D EMHD system (without hyperresistivity), and is implemented in a nonlinear MG solver. However, no grid-convergence study is offered in the reference, and relatively small implicit timesteps (of $\mathcal{O}(40)$ explicit CFLs) are used. Here, we extend the analysis to full 3D geometry (which requires dealing with the $\nabla \times \nabla \times$ operator, very challenging for geometric MG solvers), include hyperresistivity, and push implicit timesteps to 8400 CFLs without loss of algorithmic performance. The formulation is enabled by a vector-potential formulation of the HMHD system (instead of the more common magnetic-field one). The resulting smoother is able to deal seamlessly with both the whistler-wave and the fourth-order hyper-resistivity operators, both featuring $\nabla \times \nabla \times$ terms. As a result of these advances, the preconditioner renders the Jacobian-free Newton-Krylov (JFNK) solver optimally scalable algorithmically and in parallel (in a weak scaling sense) up to the largest number of processors considered in this study (16384 processors).

The rest of the paper is organized as follows. Section 2 introduces the base model equations. Sec. 3 discusses the details of the proposed physics-based preconditioner. Numerical details of our implementation, including the multigrid (MG) treatment of the hyperbolicly stiff HMHD system, are provided in Sec. 4 (with detailed analysis of the smoothing properties of our block-Jacobi treatment of the Hall MHD equations provided in Appendix A). Linear and nonlinear verification results of our implementation using wave propagation examples and the GEM challenge problem [13], respectively, along with a weak parallel

scalability study of our implicit solver up to 16384 cores, are presented in Sec. 5. Finally, we conclude in Sec. 6.

2. Vector-potential formulation of the Hall MHD model

In Alfvénic units (i.e, Alfvén speed $v_A = B_0/\sqrt{\mu_0\rho_0}$, Alfvén time $\tau_A = L/v_A$, where B_0 , ρ_0 , and L are the reference magnetic field, density, and length, respectively), the HMHD model of interest for this study reads:

$$\frac{\partial \rho}{\partial t} + \nabla \cdot (\rho \mathbf{v}) = 0, \quad (1)$$

$$\frac{\partial \mathbf{B}}{\partial t} + \nabla \times \mathbf{E} = 0 \quad (2)$$

$$\frac{\partial(\rho \mathbf{v})}{\partial t} + \nabla \cdot [\rho \mathbf{v} \mathbf{v} - \mathbf{B} \mathbf{B} + \mathbb{I}(p + \frac{B^2}{2}) + \Pi_i] = 0, \quad (3)$$

$$\frac{\partial p}{\partial t} + \nabla \cdot (\mathbf{v}^* p) + (\gamma - 1)p \nabla \cdot \mathbf{v}^* = (\gamma - 1)(Q - \nabla \cdot \mathbf{q}), \quad (4)$$

with \mathbb{I} the identity operator, ρ the particle density, \mathbf{v} the plasma velocity, \mathbf{B} the magnetic field, \mathbf{E} the electric field, $p = \rho T = (1 + \alpha)\rho T_e$ the total pressure, and $\mathbf{v}^* = \frac{\alpha \mathbf{v} + \mathbf{v}_e}{\alpha + 1} = \mathbf{v} - \frac{d_i}{1 + \alpha} \frac{\mathbf{j}}{\rho}$. Here, $\alpha = T_i/T_e$ is a fixed ion-to-electron temperature ratio, $\mathbf{v}_e = \mathbf{v} - d_i \mathbf{j}/\rho$ is the electron velocity, $\mathbf{j} = \nabla \times \mathbf{B}$ is the current, and $d_i = c/\omega_{pi}L$ the dimensionless ion inertial length. The velocity \mathbf{v}^* in the pressure equation, Eq. 4, is derived by adding the ion and electron internal energy evolution equations [26], and using the fixed-temperature-ratio assumption to ensure existence of a local energy conservation law for fixed temperature ratio α , as we outline below. Note that the pressure equation reverts to the electron pressure equation $p_e = p/(1 + \alpha)$ for cold ions ($\alpha \ll 1$), and to the ion pressure equation $p_i = p\alpha/(1 + \alpha)$ for cold electrons ($\alpha \gg 1$).

In these equations, η is the normalized resistivity (inverse Lundquist number), \mathbf{q} is the heat flux, and $Q = \eta j^2 - \sum_{s=i,e} \Pi_s : \nabla \mathbf{v}_s$ contains the joule and viscous heating sources. Simple closures for the heat flux $\mathbf{q} = -\kappa \nabla T_e$ and the viscous stress tensors $\Pi_s = -\rho \mathbf{v}_s \nabla \mathbf{v}_s$ (with s the species, and \mathbf{v}_s the normalized viscosity) are considered at this time. More accurate closures (such as gyroviscosity and anisotropic heat transport) will be considered in future work.

Key to the character of the model in Eqs. 1-4 is the specification of the electric field \mathbf{E} via an Ohm's law. In general, the Ohm's law is derived from the electron equation of motion, which reads:

$$\mathbf{E} = -\mathbf{v} \times \mathbf{B} + \eta \mathbf{j} + \frac{d_i}{\rho} (\mathbf{j} \times \mathbf{B} - \nabla p_e - \nabla \cdot \Pi_e) - \frac{d_e^2}{d_i} \frac{d \mathbf{v}_e}{dt} = -\mathbf{v}_e \times \mathbf{B} + \eta \mathbf{j} - \frac{d_i}{\rho} (\nabla p_e + \nabla \cdot \Pi_e) - \frac{d_e^2}{d_i} \frac{d \mathbf{v}_e}{dt}. \quad (5)$$

The parameter d_i characterizes the importance of Hall effects: for $d_i \ll 1$ the model transitions to resistive MHD, while for $d_i \gg 1$ the model transitions to the so-called electron MHD model [27, 28]. The parameter $d_e = c/\omega_{pe}L$ is the dimensionless electron inertial length, which characterizes the importance of electron inertia. The ion and electron inertial lengths are related as $d_e^2/d_i^2 = m_e/m_i$.

The system of Eqs. 1-4, together with Eq. 5, admits the following local energy conservation law:

$$\partial_t \left(\rho \frac{v^2}{2} + \frac{B^2}{2} + \frac{p}{\gamma - 1} \right) + \nabla \cdot \left[\rho \frac{v^2}{2} \mathbf{v} + \mathbf{E} \times \mathbf{B} + \frac{\gamma p}{\gamma - 1} \mathbf{v}^* + \sum_{s=i,e} \Pi_s \cdot \mathbf{v}_s + \mathbf{q} \right] = 0.$$

This implies that, with appropriate boundary conditions [e.g., perfect conductor ($\mathbf{E} \times \mathbf{n} = 0$), impenetrable wall ($\mathbf{v} \cdot \mathbf{n} = 0$), and no viscous stress ($\mathbf{n} \cdot \Pi_s = \mathbf{0}$)], the total energy is exactly conserved. Numerically, energy will be conserved only approximately, since we are solving for the specific internal energy (Eq. 4) instead

of total energy (the former is more advantageous for low plasma- β applications). In our simulations, energy is typically conserved to better than one part in 10^3 .

For sufficiently large d_i , the system in Eqs. 1-4, together with Eq. 5, is dispersively hyperbolic, supporting fast dispersive normal modes (Chap. 3 in Ref. [29]). In many applications of interest, however, dynamical time scales of interest are much slower than those associated with these normal modes. This is so because macroscopic dynamical time scales of interest are typically related to the bulk plasma, and thus controlled by ions, while the much faster normal modes are related to electron physics. In such instances, an implicit approach that steps over the fast normal-mode time scales to resolve the slower time scales of interest is advantageous. This is the subject of this paper. However, as we shall see, the extreme hyperbolic character of the Hall MHD model makes the task of developing an optimal, scalable solver a very difficult task.

For preconditioning purposes, we will find it advantageous to consider a governing equation for the magnetic vector potential \mathbf{A} instead of the magnetic field \mathbf{B} (which are related as $\mathbf{B} = \nabla \times \mathbf{A}$). Evolving \mathbf{A} instead of \mathbf{B} has additional benefits in that it allows more flexibility in the numerical discretization without sacrificing the solenoidal property of the magnetic field. However, it is also more challenging in that it requires a suitable gauge, and care must be taken with boundary conditions. The evolution equation for \mathbf{A} is found from $\mathbf{E} = -\nabla\Phi - \partial_t\mathbf{A}$ (where Φ is a scalar potential) and the generalized Ohm's law, Eq. 5, and reads:

$$\frac{\partial \mathbf{A}}{\partial t} + \mathbf{E} = \frac{\partial \mathbf{A}}{\partial t} - \mathbf{v}_e \times \mathbf{B} + \eta \mathbf{j} - \frac{d_i}{\rho} (\nabla p_e + \nabla \cdot \Pi_e) - \frac{d_e^2}{d_i} \frac{d \mathbf{v}_e}{dt} = -\nabla \Phi. \quad (6)$$

One can eliminate Φ by choosing an appropriate gauge. Here, we consider a variation of the Weyl gauge, $\Phi = -\frac{d_e^2}{d_i} \frac{v_e^2}{2}$, to find:

$$\frac{\partial \mathbf{A}^*}{\partial t} - \mathbf{v}_e \times (\nabla \times \mathbf{A}^*) + \eta \nabla \times \nabla \times \mathbf{A} - \frac{d_i}{\rho} (\nabla p_e + \nabla \cdot \Pi_e) = \mathbf{0}, \quad (7)$$

where $\mathbf{A}^* = \mathbf{A} - \frac{d_e^2}{d_i} \mathbf{v}_e$. This equation is what we implement numerically. The solenoidal constraint of the magnetic field is automatically guaranteed as long as $\nabla \cdot \nabla \times = 0$ discretely (as is the case in our implementation [30]). We discuss the specifics of the electron pressure tensor term in the next section.

As stated earlier, a simple viscous closure is used for both species, $\Pi_s \approx -\rho v_s \nabla \mathbf{v}_s$. It is important to note that the main purpose of keeping the electron pressure tensor contribution in our implementation, in the absence of a more informed closure, is to regularize the electron equation of motion by providing some dissipation scale. Such regularization is needed for numerical purposes, as has been described in various other studies [13, 3]. In our context, we have seen rapid degradation of the preconditioner performance when such a term is lacking. The reason is that approximations introduced in the preconditioner impact small scales the most [18], and the dispersive nature of Hall MHD seems to amplify these differences to the point that it renders the preconditioner ineffective after just a few implicit time steps.

For electrons, the simple viscous closure gives:

$$\nabla \cdot \Pi_e = -\nabla \cdot (\rho v_e \nabla \mathbf{v}_e) = -\nabla \cdot \left[\rho v_e \nabla \left(\mathbf{v} - \frac{d_i}{\rho} \mathbf{j} \right) \right] = -\nabla \cdot \left[\rho v_e \nabla \left(\mathbf{v} - \frac{d_i}{\rho} \nabla \times \nabla \times \mathbf{A} \right) \right], \quad (8)$$

where v_e is the electron viscosity (also known as hyperresistivity). This expression contains a fourth-order dissipation operator on \mathbf{A} , with $d_i \nabla \cdot \Pi_e \sim d_i^2 v_e \nabla^2 (\nabla \times \nabla \times \mathbf{A})$. The higher differential order is needed to provide a dissipation length scale to quadratic dispersive waves with dispersion relation $\omega \sim k^2$ [13]. Numerical considerations can help to determine a grid-bound v_e that provides sufficient dissipation while avoiding excessive stiffness from the high-order operators. An estimate of v_e can be obtained by balancing the damping rate $d_i^2 v_e k^4$ with the dispersive wave frequency $d_i v_A k_{\parallel} k$, to find [3]:

$$v_e = C d_i^{-1} v_A k_{\parallel} k^{-3}, \quad (9)$$

with C a constant of order unity.

We comment briefly on the discretization of Eqs. 1-4. Spatially, the system is discretized using second-order finite volumes with all variables (vectors and scalars) co-located at cell centers [30]. Such spatial representation is conservative and nonlinearly stable, and has proved to remarkably robust both in resistive [30] and Hall MHD (see Ref. [5] and results herein). Temporally, we employ either a θ -scheme with $\theta = 0.5$ (second-order Crank-Nicolson), or second-order backward differentiation formulas [31], depending on the problem. Either approach results in a set of nonlinear algebraic equations $\mathbf{G}(\mathbf{x}) = \mathbf{0}$, with $\mathbf{x}^T = (\rho, T, \mathbf{A}, \mathbf{v})$, that needs to be inverted every time step. For this, we employ preconditioned Jacobian-free Newton-Krylov (JFNK) methods. The next section discusses our approach to preconditioning the Hall MHD system.

3. Physics-based preconditioning strategy

We formulate our preconditioner by first parabolizing the implicitly discretized hyperbolic system via an approximate block factorization, and then invert the resulting systems with multigrid methods (MG) for scalability.

As preconditioners, MG methods have been shown in many applications of interest to lead to optimal convergence rates in JFNK [32]. The key element in a working MG solver is the smoother. While smoothers can be found fairly easily for diagonally dominant systems (in a point or block sense; p. 96 in [33]), it is remarkably hard otherwise. Hyperbolic systems (such as MHD) can be shown to be diagonally submissive when time steps larger than the explicit CFL stability constraint are employed (see Ref. [34] for an in-depth explanation of this issue). However, hyperbolic systems can be conveniently parabolized in an implicit time-stepping setting. The basic idea is to produce a well-conditioned (diagonally-dominant) parabolic operator from an ill-conditioned hyperbolic system of equations by a block factorization [35, 32, 36, 34, 3, 37, 18, 38, 39, 40, 41]. The procedure can be understood easily with a first-order coupled hyperbolic linear system:

$$\begin{aligned}\partial_t u &= \partial_x v, \\ \partial_t v &= \partial_x u.\end{aligned}$$

Differencing implicitly in time (with backward Euler for simplicity) but keeping the continuum spatial representation, we have:

$$u^{n+1} = u^n + \Delta t \partial_x v^{n+1}, \quad (10)$$

$$v^{n+1} = v^n + \Delta t \partial_x u^{n+1}. \quad (11)$$

It is now possible to substitute the second equation into the first to obtain the following parabolic equation:

$$(\mathbb{I} - \Delta t^2 \partial_{xx}) u^{n+1} = u^n + \Delta t \partial_x v^n, \quad (12)$$

which is equivalent to Eqs. 10-11, but much better conditioned because the parabolic operator is diagonally dominant. Once u^{n+1} is found, v^{n+1} can be found straightforwardly from Eq. 11. A similar idea is behind the method of differential approximations [42], and the semi-implicit solvers developed in the MHD context [43, 44, 1].

The parabolization of the hyperbolic equation is a manifestation of the implicit discretization of the semi-discrete hyperbolic system. Indeed, hyperbolic waves feature a finite propagation speed. By construction, implicit methods are designed to step over stiff hyperbolic waves to follow the dynamics on a slower time scale. In order to do so, the implicit scheme must change the character of the equations for unresolved hyperbolic time scales, and parabolization is the outcome. Resolved hyperbolic time scales maintain their character. This can be clearly seen from Eq. 12: for small enough time steps, the second-order term can be

neglected, and one recovers an explicit (hyperbolic) formulation. It is only for large enough time steps that the system changes character to become parabolic.

The connection between parabolization and the Schur factorization [3, 18] enables the generalization of these ideas to more complicated hyperbolic systems. Equations 10-11, when written in block-matrix form, can be factorized as:

$$\begin{bmatrix} \mathbb{I} & -\Delta t \partial_x \\ -\Delta t \partial_x & \mathbb{I} \end{bmatrix} = \begin{bmatrix} \mathbb{I} & -\Delta t \partial_x \\ 0 & \mathbb{I} \end{bmatrix} \begin{bmatrix} \mathbb{I} - \Delta t^2 \partial_x^2 & 0 \\ 0 & \mathbb{I} \end{bmatrix} \begin{bmatrix} \mathbb{I} & 0 \\ -\Delta t \partial_x & \mathbb{I} \end{bmatrix}.$$

The connection is now obvious, as the parabolic operator appears naturally. Its usefulness will become apparent in the following sections.

3.1. Block structure of the linearized Hall MHD model

We begin by considering the linearized Hall MHD model for our preconditioning development. Neglecting heat sources (which do not introduce stiff time scales), the coupling structure of the linearized MHD system in terms of the linear updates $\delta\rho$, δT_e , $\delta\mathbf{A}$, and $\delta\mathbf{v}$ reads:

$$\begin{aligned} \delta\rho &= \mathcal{L}_\rho(\delta\rho, \delta\mathbf{v}), \\ \delta p &= \mathcal{L}_T(\delta p, \delta\mathbf{v}, \delta\mathbf{A}, \delta\rho), \\ \delta\mathbf{A} &= \mathcal{L}_E(\delta\mathbf{v}, \delta\mathbf{A}, \delta\rho, \delta p), \\ \delta\mathbf{v} &= \mathcal{L}_v(\delta\mathbf{v}, \delta\mathbf{A}, \delta\rho, \delta p), \end{aligned}$$

where the \mathcal{L}_i represent linear operators. The resulting Jacobian structure is:

$$J\delta\mathbf{x} = \begin{bmatrix} D_\rho & 0 & 0 & U_{\rho v} \\ \boxed{L_{p\rho}} & D_p & \boxed{U_{p\mathbf{A}}} & U_{pv} \\ \boxed{L_{\mathbf{A}\rho}} & \boxed{L_{\mathbf{A}p}} & \boxed{D_{\mathbf{A}}} & U_{v\mathbf{A}} \\ L_{v\rho} & L_{vp} & L_{v\mathbf{A}} & D_v \end{bmatrix} \begin{pmatrix} \delta\rho \\ \delta p \\ \delta\mathbf{A} \\ \delta\mathbf{v} \end{pmatrix}. \quad (13)$$

The boxed blocks contain Hall-MHD contributions from finite d_i terms (stemming from the Ohm's law and the definition of \mathbf{v}^* in the temperature equation). Here, diagonal blocks are given by:

$$\begin{aligned} D_\rho \delta\rho &= \frac{\delta\rho}{\Delta t} + \theta[\nabla \cdot (\mathbf{v}_0 \delta\rho) - D\nabla^2 \delta\rho], \\ D_p \delta p &= \left(\frac{1}{\Delta t} + \theta(\gamma - 1)\nabla \cdot \mathbf{v}_0^* \right) \delta p + \theta[\nabla \cdot (\mathbf{v}_0^* \delta p) - \frac{\kappa}{\alpha_T \rho_0} \nabla^2 \delta T], \\ D_{\mathbf{A}} \delta\mathbf{A} &= \frac{\delta\mathbf{A}^*}{\Delta t} - \theta \left(\mathbf{v}_{e,0} \times \nabla \times \delta\mathbf{A}^* - d_i \frac{\nabla \times \nabla \times \delta\mathbf{A}}{\rho_0} \times \mathbf{B}_0 - \eta \nabla \times \nabla \times \delta\mathbf{A} + \nabla \cdot \left[\rho_0 d_i \mathbf{v}_e \nabla \left(\frac{\nabla \times \nabla \times \delta\mathbf{A}}{\rho_0} \right) \right] \right), \\ D_v \delta\mathbf{v} &= \rho_0 \left[\frac{\delta\mathbf{v}}{\Delta t} + \theta(\mathbf{v}_0 \cdot \nabla \delta\mathbf{v} + \delta\mathbf{v} \cdot \nabla \mathbf{v}_0) \right] - \theta \nabla \cdot (\mathbf{v}_i \rho_0 \nabla \delta\mathbf{v}), \end{aligned}$$

where, for D_v , we have used the non-conservative form of the momentum equation [18]. Here, θ is the time centering parameter, and $\delta\mathbf{A}^* = \delta\mathbf{A} + \frac{d_e^2}{\rho_0} \nabla \times \nabla \times \delta\mathbf{A}$. Off-diagonal blocks L and U are given by:

$$\begin{aligned} U_{\rho v} \delta\mathbf{v} &= \theta \nabla \cdot (\delta\mathbf{v} \rho_0), \\ U_{p\mathbf{A}} \delta\mathbf{A} &= -\theta d_i \left[\nabla \cdot (T_{e,0} \nabla \times \nabla \times \delta\mathbf{A}) + (\gamma - 1) p_{e,0} \nabla \cdot \frac{\nabla \times \nabla \times \delta\mathbf{A}}{\rho_0} \right], \\ U_{v\mathbf{A}} \delta\mathbf{v} &= -\theta \delta\mathbf{v} \times \mathbf{B}_0, \end{aligned}$$

$$\begin{aligned}
U_{p\mathbf{v}}\delta\mathbf{v} &= \theta[\nabla\cdot(\delta\mathbf{v}p_0) + (\gamma-1)p_0\nabla\cdot\delta\mathbf{v}], \\
L_{\mathbf{A}\rho}\delta\rho &\approx \theta d_i \frac{\delta\rho}{\rho_0^2} \nabla p_{e,0}, \\
L_{p\rho}\delta\rho &= \theta \frac{d_i}{1+\alpha} \left[\nabla\cdot\left(\frac{\delta\rho}{\rho_0^2} p_0 \mathbf{j}_0\right) + (\gamma-1)p_0\nabla\cdot\left(\frac{\delta\rho}{\rho_0^2} \mathbf{j}_0\right) \right], \\
L_{\mathbf{A}p}\delta p &= -\theta \frac{d_i}{1+\alpha} \frac{1}{\rho_0} \nabla\delta p, \\
L_{\mathbf{v}p}\delta p &= \delta\rho \left(\frac{\mathbf{v}_0}{\Delta t} + \theta \mathbf{v}_0 \cdot \nabla \mathbf{v}_0 \right) - \theta \nabla\cdot((\mathbf{v}_i + \mathbf{v}_e)\delta\rho \nabla \mathbf{v}_0), \\
L_{\mathbf{v}\mathbf{A}}\delta\mathbf{A} &= -\theta [\mathbf{j}_0 \times \nabla \times \delta\mathbf{A} + (\nabla \times \nabla \times \delta\mathbf{A}) \times \mathbf{B}_0], \\
L_{\mathbf{v}p}\delta p &= \theta \nabla\delta p.
\end{aligned}$$

3.2. Parabolization of the Hall MHD Jacobian matrix

Upon inspection of Eq. 13, it is clear that the convenient ‘‘arrow structure’’ of the resistive MHD Jacobian matrix [18] has been spoiled. However, the stiff electron timescales introduced in Hall MHD are all contained in the magnetic field diagonal block $D_{\mathbf{A}}$ via the $d_i(\frac{\nabla \times \nabla \times \delta\mathbf{A}}{\rho_0} \times \mathbf{B}_0)$ term, responsible for the propagation of fast whistler waves. This realization opens the way for a tractable physics-based preconditioning algorithm.

The Jacobian recovers a manageable structure by simply neglecting the block $U_{p\mathbf{A}}$ (stemming from the linearization of the current correction in the \mathbf{v}_s velocity, which is not stiff). Then, the approximate Jacobian system reads:

$$J\delta\mathbf{x} \approx \begin{bmatrix} M & U \\ L & D_{\mathbf{v}} \end{bmatrix} \begin{pmatrix} \delta\mathbf{y} \\ \delta\mathbf{v} \end{pmatrix},$$

where $\delta\mathbf{y} = (\delta\rho, \delta\mathbf{A}, \delta p)^T$, and

$$M \approx \begin{pmatrix} D_{\rho} & 0 & 0 \\ L_{p\rho} & D_p & 0 \\ L_{\mathbf{A}\rho} & L_{\mathbf{A}p} & D_{\mathbf{A}} \end{pmatrix} \quad (14)$$

a lower triangular system. The exact Schur factorization of the inverse of the 2×2 block Jacobian matrix yields:

$$\begin{bmatrix} M & U \\ L & D_{\mathbf{v}} \end{bmatrix}^{-1} = \begin{bmatrix} \mathbb{I} & -M^{-1}U \\ 0 & \mathbb{I} \end{bmatrix} \begin{bmatrix} M^{-1} & 0 \\ 0 & P_{Schur}^{-1} \end{bmatrix} \begin{bmatrix} \mathbb{I} & 0 \\ -LM^{-1} & \mathbb{I} \end{bmatrix},$$

where $P_{Schur} = D_{\mathbf{v}} - LM^{-1}U$ is the Schur complement, which contains all the information from the off-diagonal blocks L and U (similarly to the simple coupled-wave-equation example discussed earlier). This gives the *exact* inversion process:

$$\begin{aligned}
\delta\mathbf{y}^* &= -M^{-1}\mathbf{G}_y, \\
\delta\mathbf{v} &= P_{Schur}^{-1}[-\mathbf{G}_v - LM^{-1}\delta\mathbf{y}^*], \\
\delta\mathbf{y} &= \delta\mathbf{y}^* - \Delta t M^{-1}U\delta\mathbf{v}.
\end{aligned} \quad (15)$$

As it stands, however, inverting P_{Schur} is impractical due to the presence of M^{-1} . Suitable simplifications have been proposed for small ion flows [18], and later generalized to arbitrary ion flows [8], which cannot yet be directly applied in this context owing to the presence of the very stiff vector-potential diagonal block, $D_{\mathbf{A}}$. However, progress can be made by realizing that the vector potential diagonal block is the only one supporting stiff EMHD physics, while the rest of the algorithm in Eq. 15 is correcting for ion dynamics.

Since electron Hall physics is largely decoupled from ions, we hypothesize that an operator-split approach in which the electrons response is solved for first, followed by an ion response correction will form the basis for an effective preconditioner.

Making this approximation explicit in Eq. 15, we perform a full solve of M^{-1} in the first step, while in subsequent ones we neglect electron dynamics and approximate $M^{-1} \approx \Delta t \mathbb{I}$ (small-bulk-flow approximation [18]). The resulting approximate “physics-based” preconditioner reads:

$$\begin{aligned}\delta \mathbf{y}^* &= -M^{-1} \mathbf{G}_y, \\ \delta \mathbf{v} &= P_{SF}^{-1} [-\mathbf{G}_v - L \delta \mathbf{y}^*], \\ \delta \mathbf{y} &= \delta \mathbf{y}^* - \Delta t U \delta \mathbf{v},\end{aligned}\tag{16}$$

with $P_{SF} = D_v - \Delta t LU$. This is formally identical to the resistive MHD preconditioner proposed in [18], except now the inversion of the M block contains the EMHD block, which is the stiffest in the system and whose treatment we discuss in detail below. As in the reference, taking L and U from the linearized form of Eqs. 1-4, using the non-conservative form of Eq. 3, and Picard-linearizing the density (by ignoring $\delta \rho$ terms), the operator P_{SF} acting on $\delta \mathbf{v}$ reads:

$$P_{SF} \delta \mathbf{v} = \left[\rho_0 \frac{\delta \mathbf{v}}{\Delta t} + \theta \rho_0 (\mathbf{v}_0 \cdot \nabla \delta \mathbf{v} + \delta \mathbf{v} \cdot \nabla \mathbf{v}_0) - \theta \nabla \cdot (\rho_0 \mathbf{v}_i \nabla \delta \mathbf{v}) \right] + \Delta t \theta^2 W(\mathbf{B}_0, p_0) \delta \mathbf{v},\tag{17}$$

where $W(\mathbf{B}_0, p_0)$ results from the composition of off-diagonal operators L_{Av} and U_{vA} , and reads:

$$W(\mathbf{B}_0, p_0) \delta \mathbf{v} \approx \mathbf{B}_0 \times \nabla \times \nabla \times [\delta \mathbf{v} \times \mathbf{B}_0] - \mathbf{j}_0 \times \nabla \times [\delta \mathbf{v} \times \mathbf{B}_0] - \nabla [\delta \mathbf{v} \cdot \nabla p_0 + \gamma p_0 \nabla \cdot \delta \mathbf{v}],\tag{18}$$

with $\mathbf{j}_0 = \nabla \times \mathbf{B}_0$. This is a linearized form of the MHD energy principle, which is self-adjoint when $\mathbf{j}_0 \times \mathbf{B}_0 = \nabla p_0$ (and therefore has real eigenvalues in that case). Thus, the MHD system has been effectively parabolized.

Equations 16, with M defined in Eq. 14, is the proposed preconditioner. It reuses most of the elements of the resistive MHD preconditioner proposed in Ref. [18], except for the treatment of the vector potential diagonal block, which we discuss next.

4. Numerical implementation

We employ a Newton-FGMRES (flexible GMRES [23]) nonlinear iterative method, implemented Jacobian-free. Newton nonlinear convergence is controlled in our implementation by the usual criterion:

$$\|\mathbf{G}(\mathbf{x}_k)\|_2 < \varepsilon_a + \varepsilon_r \|\mathbf{G}(\mathbf{x}_0)\|_2 = \varepsilon_t,\tag{19}$$

where $\|\cdot\|_2$ is the L_2 -norm (euclidean norm), $\varepsilon_a = \sqrt{N} \times 10^{-15}$ (with N the total number of degrees of freedom) is an absolute tolerance to avoid converging below round-off, ε_r is the Newton relative convergence tolerance (set to 10^{-3} in this work), and $\mathbf{G}(\mathbf{x}_0)$ is the initial residual. GMRES convergence is controlled by an inexact Newton method [45] in which the Krylov convergence tolerance every Newton iteration is adjusted as follows:

$$\|J_k \delta \mathbf{x}_k + \mathbf{G}(\mathbf{x}_k)\|_2 < \zeta_k \|\mathbf{G}(\mathbf{x}_k)\|_2\tag{20}$$

where ζ_k is the inexact Newton parameter and $J_k = \left. \frac{\partial \mathbf{G}}{\partial \mathbf{x}} \right|_k$ is the Jacobian matrix. Here, we employ the same prescription for ζ_k as in earlier studies [3, 18]:

$$\begin{aligned}\zeta_k^A &= \gamma \left(\frac{\|\mathbf{G}(\mathbf{x}_k)\|_2}{\|\mathbf{G}(\mathbf{x}_{k-1})\|_2} \right)^\alpha, \\ \zeta_k^B &= \min[\zeta_{max}, \max(\zeta_k^A, \gamma \zeta_{k-1}^\alpha)], \\ \zeta_k &= \min[\zeta_{max}, \max(\zeta_k^B, \gamma \frac{\varepsilon_t}{\|\mathbf{G}(\mathbf{x}_k)\|_2})],\end{aligned}$$

with $\alpha = 1.5$, $\gamma = 0.9$, and $\zeta_{max} = 0.8$. The convergence tolerance ε_t is the same as in Eq. 19. In this prescription, the first step ensures superlinear convergence (for $\alpha > 1$), the second avoids volatile decreases in ζ_k , and the last avoids oversolving in the last Newton iteration.

Our geometric MG solver is fully parallel, with coarse-grid parallel domain agglomeration [24, 25]. It features a matrix-light implementation [3, 18], in which only the diagonal of the system of interest is stored for smoothing purposes. Coarse operators are found via rediscrretization, and required residuals in the MG iteration are found in a matrix-free manner. As a smoother, we employ three passes of damped Jacobi (p. 10 in [46]; p. 118 in [33]), with weight $\omega = 0.7$, for both the restriction and the prolongation steps. MG restriction employs conservative agglomeration, and prolongation employs a first-order interpolation. In MG jargon, such V-cycle is identified as V(3,3), where the two integers indicate restriction and prolongation smoothing steps, respectively. In parallel, we use colored damped Jacobi, which parallelizes very well; four colors are needed in 2D (for a 9-point stencil), and 8 colors in 3D (for a 27-point stencil). Our matrix-light geometric-MG approach features excellent parallel performance, with wall-clock time scaling logarithmically with the number of MPI tasks (as demonstrated in the next section).

For typical timesteps in HMHD, a single V(3,3) MG V-cycle is sufficient to approximately invert the diagonal blocks D_ρ , D_p , and P_{SF} in Eq. 16. However, the EMHD block D_A is much more challenging to invert robustly. For this block, we use MG-preconditioned GMRES, converged to either 10 Krylov iterations or a relative tolerance of 0.1, whichever comes first (note that nested GMRES solves in the preconditioner are allowed by FGMRES). This strategy still requires a working MG solver for the EMHD block, which in turn requires a suitable smoother. We describe our smoothing strategy for this block next.

4.1. Smoothing of the vector-potential diagonal block

In order to make the D_A operator MG-friendly we need to provide a suitable smoother. Here, we are seeking to use damped block-Jacobi smoothing, which is cheap and easily parallelizable. The D_A diagonal block contains fast electron hyperbolic physics (whistler waves, with dispersion relation $\omega \sim d_i v_A k k_{\parallel}$), electron inertia, and electron viscosity (also known as hyperresistivity), and reads:

$$D_A \delta \mathbf{A} = \frac{\delta \mathbf{A}^*}{\Delta t} - \theta \left(\mathbf{v}_{e,0} \times \nabla \times \delta \mathbf{A}^* - d_i \underbrace{\frac{\nabla \times \nabla \times \delta \mathbf{A}}{\rho_0} \times \mathbf{B}_0}_{\text{Whistler term}} - \eta \nabla \times \nabla \times \delta \mathbf{A} + \nabla \cdot \underbrace{\left[\rho_0 d_i^2 \mathbf{v}_e \nabla \left(\frac{\nabla \times \nabla \times \delta \mathbf{A}}{\rho_0} \right) \right]}_{\text{Hyperresistivity term}} \right),$$

with:

$$\delta \mathbf{A}^* = \delta \mathbf{A} + \frac{d_e^2}{\rho_0} \nabla \times \nabla \times \delta \mathbf{A}.$$

This operator is the linearized form of the EMHD model.

The iterative solution of the vector-potential diagonal block is extremely challenging, and has in fact been the key roadblock overcome in this research. It is a stiff, high differential order, vectorial system of equations. It supports fast (quadratic) dispersive waves, and features a fourth-order dissipative operator of the form $\nabla^2(\nabla \times \nabla \times)$ that provides a dissipation length scale to the fast dispersive waves, needed for nonlinear stability of the discretization [13]. The form of the dissipative operator is not only problematic because of its high order, but also because it features an infinitely degenerate null space: any gradient component in the vector potential will get annihilated by the curl. Although the D_A operator in aggregate is non-singular, the presence of a null space in the hyperresistivity term makes its MG implementation problematic. One may consider approximating it, but being the term with the highest differential order, our experience is that any approximations introduced to it will negatively (and significantly) impact the

performance of the preconditioner. In particular, replacing $\nabla \times \nabla \times$ by $-\nabla^2$ is not justified in principle because we do not use the Coulomb gauge ($\nabla \cdot \mathbf{A} = 0$) but a modified Weyl gauge, as discussed earlier. (A Coulomb gauge could in principle be used, but it would result in an additional equation for the electrostatic potential, which the Weyl gauge avoids.)

To provide for a suitable smoother, we begin by reformulating the EMHD system by splitting it into two second-order vectorial systems:

$$\begin{aligned} \frac{1}{\Delta t} \left(\delta \mathbf{A} + d_e^2 \frac{\delta \mathbf{j}}{\rho_0} \right) - \theta \left(\mathbf{v}_{e,0} \times \nabla \times \left(\delta \mathbf{A} + d_e^2 \frac{\delta \mathbf{j}}{\rho_0} \right) - d_i \frac{\delta \mathbf{j}}{\rho_0} \times \mathbf{B}_0 - \eta \delta \mathbf{j} + \nabla \cdot \left[\rho_0 d_i^2 \mathbf{v}_e \nabla \left(\frac{\delta \mathbf{j}}{\rho_0} \right) \right] \right) &= \mathbf{rhs}, \\ \delta \mathbf{j} - \nabla \times \nabla \times \delta \mathbf{A} &= \mathbf{Q21} \end{aligned}$$

The auxiliary variable $\delta \mathbf{j}$ is a physical quantity (current density), with a well-defined set of boundary conditions, ensuring the split system is well posed. The feasibility of this physical system splitting without approximation is, in fact, the key reason why we pursued a vector-potential-based representation of our Hall MHD model instead of a magnetic-field-based one. For the latter, the hyperresistivity term would read:

$$\nabla \times \nabla \cdot \left[\rho_0 d_i^2 \mathbf{v}_e \nabla \left(\frac{\nabla \times \delta \mathbf{B}}{\rho_0} \right) \right],$$

which *cannot* be split into two second-order systems in an obvious way.

The Jacobi smoother for the coupled system in Eq. 21 iterates on all local vector components for $\delta \mathbf{A}$ and $\delta \mathbf{j}$ simultaneously on a per-cell basis. To deal with the $\nabla \times \nabla \times$ operator in the smoothing stage, we employ a defect-correction approach whereby we selectively approximate $\nabla \times \nabla \times$ by $-\nabla^2$ in the computation of the diagonal blocks, but retain the $\nabla \times \nabla \times$ form for all the residual computations within the MG V-cycle. We show in the Appendix for the special case of a homogeneous plasma that this strategy produces a convergent damped-Jacobi iteration with the smoothing property (critical for the effectiveness of MG), and therefore provides an excellent basis for an effective MG preconditioner.

5. Numerical results

We have implemented this algorithm in the PIXIE3D nonlinear MHD code [30, 18, 8]. In what follows, we present numerical examples that demonstrate the correctness of our implementation as well as its performance (algorithmically and in parallel). We consider both linear examples (wave propagation) and nonlinear examples (with the well-known GEM challenge magnetic reconnection problem [13], which we verify against the HiFi nonlinear MHD code [47]). The latter example is also considered for the algorithmic and parallel performance assessment. The GEM challenge problem benefits from an implicit treatment, since the dynamical time scale of interest is independent of the grid resolution, and much slower than fast HMHD normal modes.

5.1. Linear verification: whistler wave

We consider a collisionless, homogeneous, adiabatic ($\gamma = 1$) plasma with $\rho_0 = 1$, $T_{i0} = T_{e0} = 1$, $\mathbf{B}_0 = (1, 0, 0)$, $\mathbf{v} = \mathbf{0}$, and $d_i = 10$ in a one-dimensional domain with $L_x = 1$. Linear theory predicts that the frequency of the resulting wave is $\omega = \pm d_i k_x^2$, with mode structure:

$$\begin{aligned} \delta A_y &= -i \delta A_z, \\ \omega \delta v_y &= k_x^2 \delta A_y, \\ \omega \delta v_z &= k_x^2 \delta A_z. \end{aligned}$$

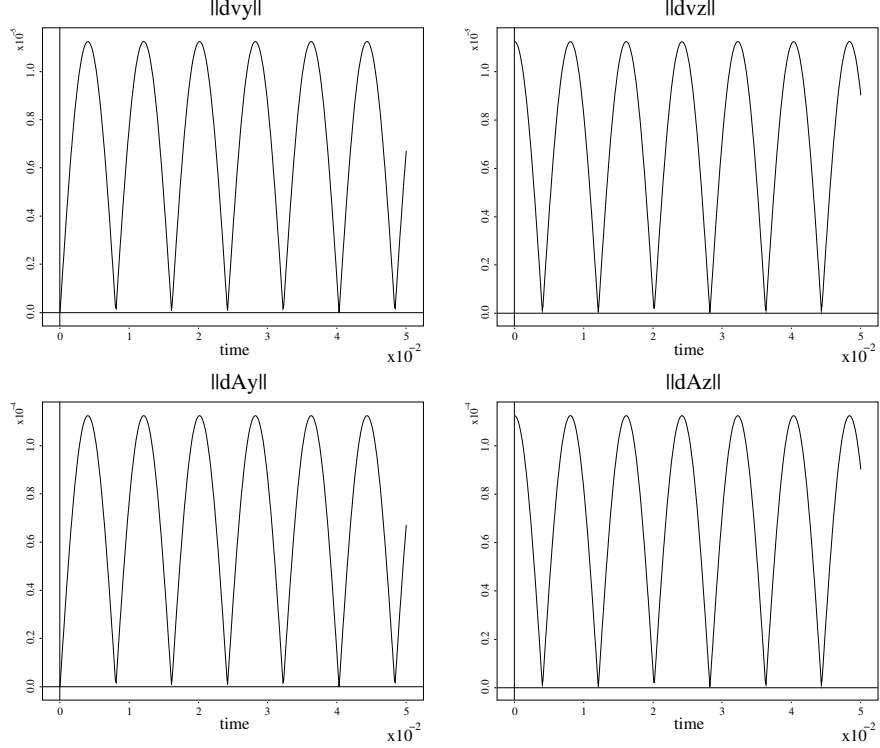


Figure 1: Time histories of perturbations of v_y , v_z , A_y , A_z for the whistler wave linear verification test.

For $k_x = 2\pi/L_x = 2\pi$, the wave period is $T = 2\pi/\omega = (2\pi d_i)^{-1} \approx 0.016$. We set up a standing whistler wave with a perturbation of the form:

$$\begin{aligned}\delta A_z &= -\frac{\varepsilon}{k_x} \sin(k_x x), \\ \delta v_z &= \frac{\varepsilon}{k_x d_i} \sin(k_x x),\end{aligned}$$

with $\varepsilon = 10^{-3}$. Simulations are performed using 32 mesh points and $\Delta t = 10^{-4}$. Figure 1 shows the time histories of the ℓ_2 -norm of δv_y , δv_z , δA_y , δA_z , where one can appreciate that, as expected: 1) wave period is 0.016, 2) $\|\delta v_y\|$ and $\|\delta A_y\|$ are in phase, as are $\|\delta v_z\|$ and $\|\delta A_z\|$, and 3) $\|\delta A_y\|$ and $\|\delta A_z\|$ are 90 degrees out of phase (as are $\|\delta v_y\|$ and $\|\delta v_z\|$).

5.2. Linear verification: kinetic Alfvén wave

We consider a collisionless, homogeneous, adiabatic ($\gamma = 1$) plasma with $\rho_0 = 1$, $T_{i0} = T_{e0} = 2.5 \times 10^3$, $\mathbf{B}_0 = (1, 0, 0)$, $\mathbf{v} = \mathbf{0}$, and $d_i = 5/\pi$ in a two-dimensional domain with $L_x = 10$ and $L_y = 1$. Linear theory predicts that the frequency of the resulting wave is $\omega \approx \pm \rho_s k_x k_y$, with $\rho_s = d_i \sqrt{\beta}/2$ the sound Larmor radius and $\beta = 2\mu_0 p_0/B_0^2 = 10^4$ the plasma beta, and mode structure:

$$\delta A_z = \frac{i}{\rho_s k_x^2} \delta v_y, \quad (22)$$

$$\delta v_y = \frac{k_x}{k_y} [d_i^2 (k_x^2 + k_y^2) - 1] \delta v_x. \quad (23)$$

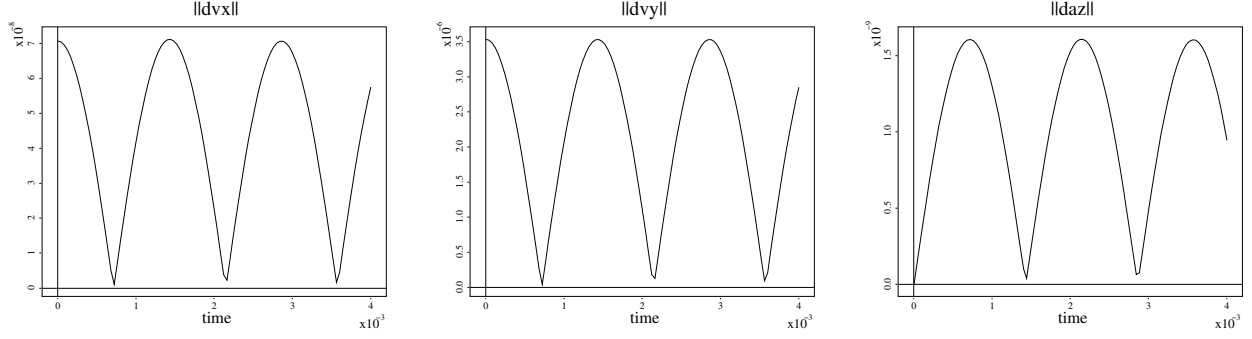


Figure 2: Time histories of perturbations of v_x , v_y , A_z for the KAW wave linear verification test.

For $k_x = 2\pi/L_x = \pi/5$, $k_y = 2\pi n_y/L_y = 2\pi n_y$, and $n_y = 5$, the wave period is $T = 2\pi/\omega = n_y^{-1}\sqrt{2/\beta} \approx 2.83 \times 10^{-3}$. We set up a standing wave with a perturbation of the form:

$$\begin{aligned}\delta v_x &= \varepsilon \cos(k_x x + k_y y), \\ \delta v_y &= \varepsilon \frac{k_x}{k_y} [d_i^2 (k_x^2 + k_y^2) - 1] \cos(k_x x + k_y y),\end{aligned}$$

with $\varepsilon = 10^{-7}$. Simulations are performed using 32×128 mesh points and $\Delta t = 4 \times 10^{-5}$. Figure 1 shows the time histories of the ℓ_2 -norm of δv_y , δv_z , δA_y , δA_z , where one can appreciate that, as expected: 1) wave period is $\approx 2.8 \times 10^{-3}$, 2) $\|\delta v_x\|$ and $\|\delta v_y\|$ are in phase and the ratio in magnitude is $\delta v_y/\delta v_x \approx 50$ (as expected from Eq. 23), and 3) $\|\delta A_z\|$ is 90 degrees out of phase from the velocity perturbations, and consistent in magnitude with Eq. 22.

5.3. Nonlinear verification: GEM challenge magnetic reconnection problem

We consider the GEM challenge problem [13] for a nonlinear verification study against the HiFi nonlinear extended MHD code. HiFi [47] is a highly accurate, fully implicit, spectral-element-based nonlinear extended MHD code. To preserve smoothness during the simulation, HiFi features a moving mesh strategy based on a Laplace-Beltrami mesh governing equation (see Ref. [48] and references therein). For consistency with HiFi, we have replaced \mathbf{v}^* in Eq. 4 with \mathbf{v} .

The GEM challenge problem setup is a Harris current sheet, defined by the vector potential $(0, 0, A_z)$, with:

$$A_z = -\lambda \ln(\cosh(x/\lambda)),$$

with $\lambda = 0.5 d_i$, balanced by a pressure profile given by constant ion and electron temperatures with $T_i/T_e = \alpha = 5$ and $(T_i + T_e) = 1/2$, and density profile:

$$\rho(x) = \frac{n_0}{\cosh(x/\lambda)} + n_\infty.$$

with $n_0 = 1$, $n_\infty = 0.2$. We consider a slab domain $(-L_x/2, L_x/2) \times (-L_y/2, L_y/2)$ with $L_x = 12.8 d_i$ and $L_y = 25.6 d_i$. Boundary conditions are perfect conductor at $\pm L_x/2$, and periodic at $\pm L_y/2$. The transport coefficients are: $v_i = 5 \times 10^{-2}$, $v_e = 10^{-4}$, $\eta = 5 \times 10^{-3}$, and $\kappa = 2 \times 10^{-2}$. The specific heat ratio is $\gamma = 5/3$.

The simulation in both codes is started by perturbing A_z with a sinusoidal perturbation of the form:

$$\delta A_z = -\varepsilon \cos\left(\frac{\pi x}{L_x}\right) \cos\left(\frac{2\pi y}{L_y}\right),$$

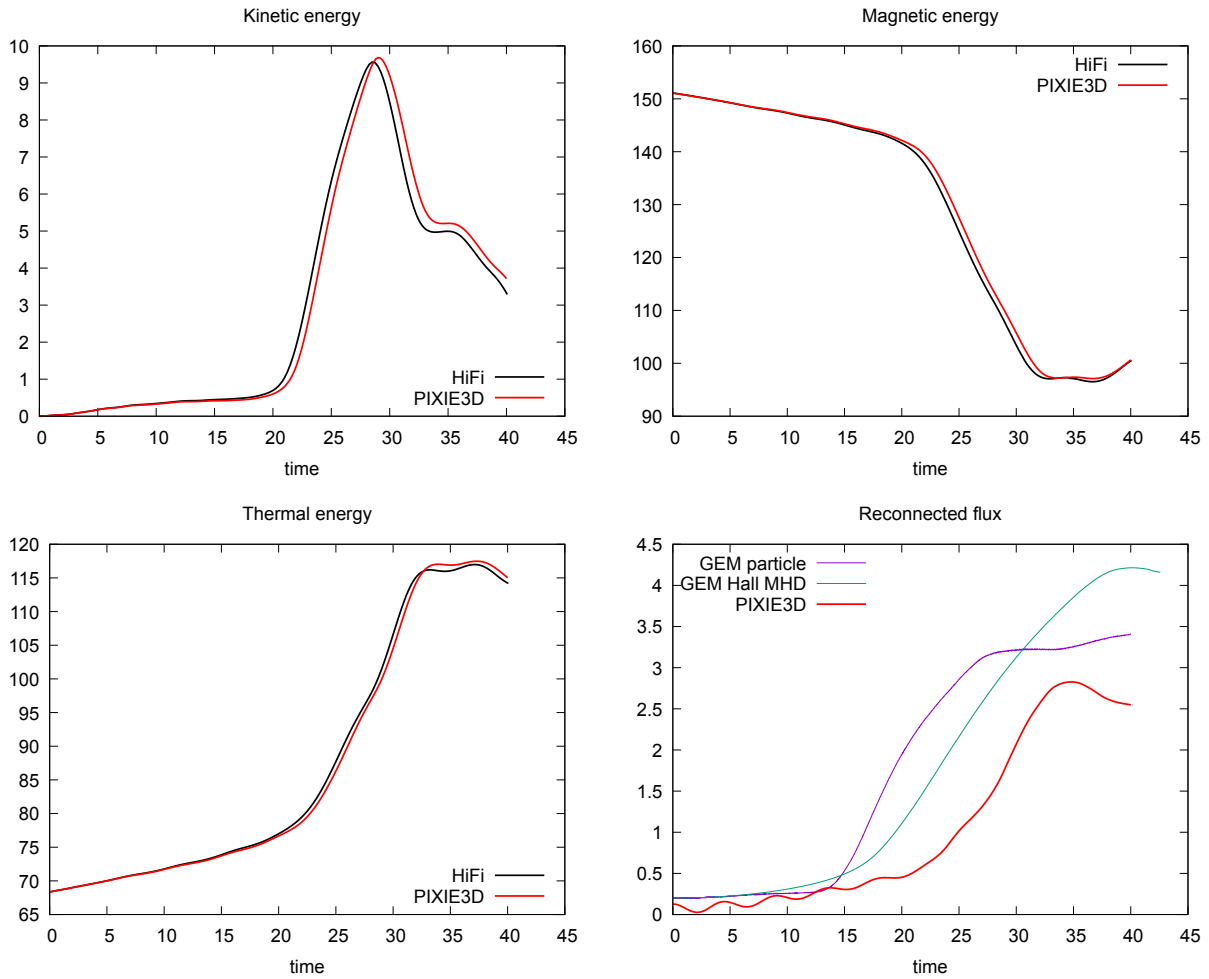


Figure 3: Nonlinear comparison of the temporal evolution of the kinetic, magnetic and thermal energies from the PIXIE3D and HiFi codes for the GEM challenge (see text for setup). The reconnected flux for PIXIE3D is compared with data from Fig. 1 of Ref. [13], with excellent agreement in the slope of the curve (which determines the peak reconnection rate) vs. the GEM results.

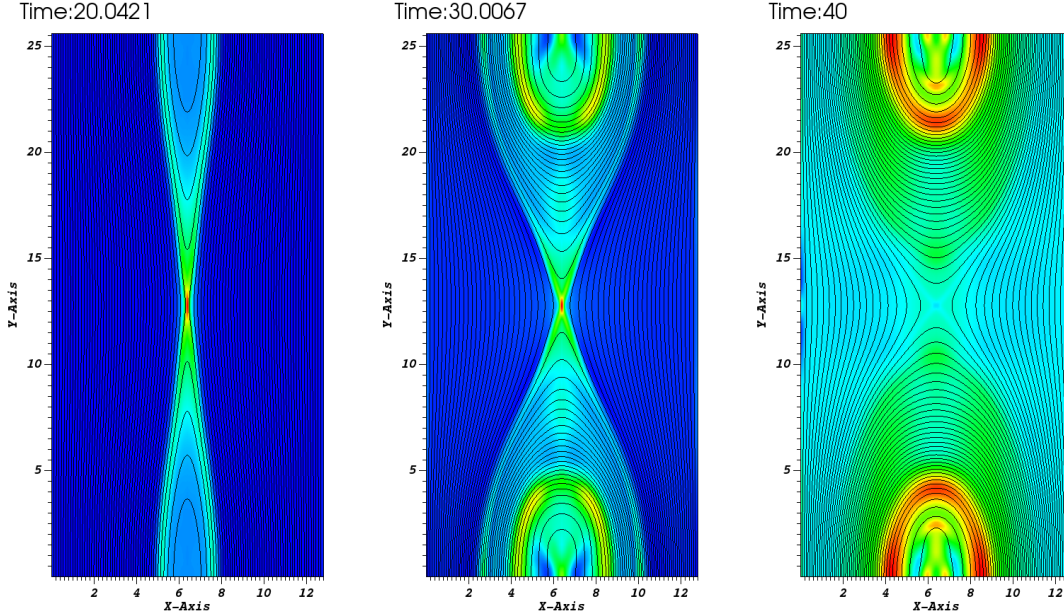


Figure 4: Snapshots of A_z (contours) and j_z (color) at three different times ($t = 20, 30, 40$) for the GEM simulation.

with $\varepsilon = 10^{-1}$. This problem was run with a 256×256 packed mesh along both axes, with $\Delta x = 2 \times 10^{-2}$ at $x = 0$ (at the rational surface), and $\Delta y = 5 \times 10^{-2}$ at $y = \pm L_y/2$ (the periodic boundaries). This represents a packing ratio vs. the uniform mesh of 2.5 in x and 2 in y . The time step is $\Delta t = 0.05$.

In addition to the reconnected flux (which is a robust measure [13]), we also track the temporal histories of kinetic ($\frac{1}{2} \int d\mathbf{x} \rho v^2$), magnetic ($\frac{1}{2} \int d\mathbf{x} B^2$), and thermal ($\frac{1}{2} \int d\mathbf{x} \frac{p}{\gamma-1}$) energies, which are more nuanced. The time history comparison is depicted in Fig. 3, and shows an early (slow) phase followed by a late, explosive phase characterized by rapid growth of kinetic energy and thermal energy, fed by a significant decrease in magnetic energy. During this evolution, total energy is conserved better than 0.04%. The comparison shows remarkably good agreement between HiFi and PIXIE3D during the slow phase and most of the explosive phase, with some deviation (of about 1%) late in the nonlinear evolution of the problem. Key elements of comparison are the excellent agreement in the timing of the transition from slow to explosive phase, in the slopes during most of the explosive phase, and in the extrema values of the energies at saturation. The reconnected flux for PIXIE3D is also shown, along with data from Ref. [13] for the fully kinetic particle simulation and the Hall MHD simulation. While details differ in terms of timing and saturation level, the agreement in the slope (maximum reconnection rate) between all three simulations is apparent. The reconnected-flux history itself is not, but it is in very good qualitative agreement with more recent HMHD GEM results, e.g. Fig. 13 of Ref. [49].

Snapshots of the z -component of the vector potential and the current density for the GEM challenge at $t = 20$ (before the explosive phase), $t = 30$ (at the peak of the explosive phase), and $t = 40$ (at the end of the simulation) are depicted in Fig. 4. The formation of an open X-point and associated current density spike is apparent. We do not find the formation of a central magnetic island for our particular choice of parameters, which has been the subject of contention in the literature [10, 17].

5.4. Parallel and algorithmic performance

We assess the (weak) parallel and algorithmic scalability of our solver with the GEM challenge problem, with slightly modified parameters as indicated below. Preconditioner setup and linear and nonlinear convergence tolerances are set as stated earlier. For this exercise, we consider uniform meshes in full domain starting at 32×32 with $n_p = 1$ MPI task, up to 4096×4096 meshes with $n_p = 16384$ tasks. We consider a

Table 1: Parallel weak-scaling performance for the GEM Challenge problem with $\Delta t = 0.01$ and $\eta = \nu_i = \kappa = 5 \times 10^{-4}$. Results are obtained in full domain and a uniform Cartesian mesh, and averaged over 100 time steps with a fixed timestep $\Delta t = 0.01$. In this table, WCT stands for wall-clock time. Speedup measures the speedup vs and explicit method.

n_p	mesh	ν_e	$\frac{\Delta t}{\Delta t_{exp}}$	GMRES/ Δt	Newton/ Δt	WCT(s)	WCT/GMRES	Speedup
1	32×32	10^{-4}	1.0	2.0	2.0	132	66	0.04
4	64×64	2.5×10^{-5}	2.1	2.6	2.6	172	66	0.07
16	128×128	6.3×10^{-6}	8.3	2.0	2.0	182	105	0.26
64	256×256	1.6×10^{-6}	33	2.0	2.0	303	151	0.63
256	512×512	3.9×10^{-7}	130	2.0	2.0	321	160	3.0
1024	1024×1024	9.8×10^{-8}	520	2.0	2.0	509	203	8.5
4096	2048×2048	2.4×10^{-8}	2100	2.0	2.0	512	256	38
16384	4096×4096	6.0×10^{-9}	8400	3.0	3.0	1130	377	75

fixed implicit timestep ($\Delta t = 0.01$) for all experiments, so the problem is becoming numerically stiffer as the number of MPI tasks grows. In this way, when increasing the processor count we are able to test the ability of the algorithm to *both* scale with mesh refinement and to scale in parallel. To maintain the simulation in the stiff hyperbolic regime, we decrease the hyperresistivity coefficient as we refine the mesh according to Eq. 9 to ensure that high-order dissipation is only provided for the grid-scale components of the solution.

The results of the mesh/processor convergence study are shown in Table 1. Timings have been obtained on the CPU partition of the Chicoma computer at Los Alamos National Laboratory, featuring 1792 nodes, each with two Rome 64 core 2.6 GHz CPUs (also called the AMD EPYC 7H12) with 512 GB per node. Several observations are in order. Firstly, as advanced earlier, the fixed implicit timestep results in a stiffer numerical setup as we refine the mesh, and indicated by the increase in $\Delta t/\Delta t_{exp}$ (with Δt_{exp} the explicit stability-limit CFL timestep). Next, the total number of GMRES iterations per timestep (GMRES/ Δt , which includes all Newton iterations) shows a very weak dependence with mesh resolution (and number of MPI tasks), attesting to the effectiveness of our preconditioning strategy. The performance of our MG parallel implementation is demonstrated by the WCT/GMRES column, which measures the time per GMRES iteration, which is dominated by the MG preconditioning step and features a $\log(n_p)$ increase. The favorable algorithmic (per the GMRES/ Δt column) and parallel (per the WCT/GMRES column) scalings result in an overall remarkable scaling of the wall-clock time WCT, which only increases by a factor of 8.6 when increasing the problem size by a factor of 16384. It also results in a speedup of 75 for the finest mesh considered vs. an explicit integrator, with performance cross-over between implicit and explicit happening at moderate meshes (between 256×256 and 512×512 ; the cross-over happens at such fine meshes due to the fairly conservative solver-parameter choices of the MG solver for the inversion of the EMHD block, which makes the preconditioner quite expensive).

6. Conclusions

We have developed a parallel, scalable multigrid-based physics-based preconditioning strategy for the Hall MHD equation system. As in earlier MHD preconditioning studies, the physics-based preconditioning approach exploits the natural parabolization of the hyperbolic couplings that occurs when one discretizes them implicitly. The block structure of the Hall MHD Jacobian spoils the ‘‘arrow’’ structure that was so convenient in resistive MHD, but can still be formally Schur-factorized in much the same way leading to a coupled system of equations for the fluid velocity components. The Schur factorization is rendered practical by 1) using the small-bulk-flow approximation (as in earlier studies), and 2) exploiting the natural separation of stiff timescales between ions and electrons in Hall MHD to segregate the electromagnetic diagonal block solve.

The electromagnetic diagonal block corresponds to the so-called electron MHD model (EMHD), and supports fast (quadratic) dispersive waves and high-order dissipation (hyperresistivity), which is critical for nonlinear stability. We invert this system robustly and scalably with MG-preconditioned GMRES (nested GMRES solves in the preconditioning stage are allowed by FGMRES in JFNK). Several strategies have helped in rendering the EMHD block MG-friendly. Firstly, we have chosen to solve the vector-potential formulation of Hall MHD (instead of the more standard magnetic field one), which allowed us to reformulate the EMHD block into a set of two coupled vectorial equations with physical interpretation (vector potential and current density, respectively) and well-defined boundary conditions. This coupled set of equations is Jacobi-smoothed in a fully coupled manner. Secondly, we use a deferred-correction approach in our MG smoothing strategy, whereby we approximate the $\nabla \times \nabla \times$ operator (which relates the current density and the vector potential) as a vector Laplacian for the construction of the Jacobi block diagonals. This strategy is demonstrated by analysis to produce a strongly smoothing damped Jacobi iteration, and therefore a robust MG algorithm.

We have verified our implementation linearly with two wave propagation tests, a whistler wave and a KAW, and nonlinearly with the GEM challenge problem, by direct comparison with the HiFi spectral extended MHD code. We have demonstrated the excellent scalability properties of our preconditioner algorithmically (by demonstrating a bounded iteration count with grid refinement) and in parallel (by demonstrating logarithmic scaling of wall clock time with the number of MPI tasks in a weak scaling sense with up to 16384 processors).

Future work will focus on extending the algorithm to singular coordinate systems (with application to cylindrical and toroidal geometries, of interest for fusion plasma simulation), and to include separate ion and electron temperatures, anisotropic heat transport, and gyroviscosity.

Acknowledgments

We acknowledge useful discussions with J. N. Shadid and A. Stanier. We also acknowledge V. Lukin for providing the GEM challenge simulation data for comparison with the HiFi code. This work was supported by Triad National Security, LLC under contract 89233218CNA000001 and DOE Office of Applied Scientific Computing Research (ASCR). The research used computing resources provided by the Los Alamos National Laboratory Institutional Computing Program.

References

- [1] D. S. Harned and Z. Mikic, “Accurate semi-implicit treatment of the Hall effect in magnetohydrodynamic computations,” *J. Comput. Phys.*, vol. 83, pp. 1–15, 1989.
- [2] C. R. Sovinec, J. R. King, and NIMROD Team, “Analysis of a mixed semi-implicit/implicit algorithm for low-frequency two-fluid plasma modeling,” *J. Comput. Phys.*, vol. 229, pp. 5803–5819, AUG 10 2010.
- [3] L. Chacón and D. A. Knoll, “A 2D high- β Hall MHD implicit nonlinear solver,” *J. Comput. Phys.*, vol. 188, no. 2, pp. 573–592, 2003.
- [4] S. C. Jardin and J. A. Breslau, “Implicit solution of the four-field extended-magnetohydrodynamic equations using high-order high-continuity finite elements,” *Phys. Plasmas*, vol. 12, no. 5, p. 056101, 2005.
- [5] K. Germaschewski, A. Bhattacharjee, and C.-S. Ng, “The Magnetic Reconnection Code: an AMR-based fully implicit simulation suite,” in *Numerical Modeling of Space Plasma Flows* (N. B. Pogorelov and G. P. Zank, eds.), vol. 359 of *ASP Conference Series*, p. 151, 2006.

- [6] S. Ovtchinnikov, F. Dobrian, X.-C. Cai, and D. Keyes, “Additive schwarz-based fully coupled implicit methods for resistive hall magnetohydrodynamic problems,” *J. Comput. Phys.*, vol. 225, pp. 1919 – 1936, 2007.
- [7] L. Chacon and A. Stanier, “A scalable, fully implicit algorithm for the reduced two-field low- β extended mhd model,” *Journal of Computational Physics*, vol. 326, pp. 763–772, 2016.
- [8] L. Chacón, “Scalable solvers for 3D magnetohydrodynamics,” *J. Physics: Conf. Series*, vol. 125, p. 012041, 2008.
- [9] L. Arnold, J. Dreher, and R. Grauer, “A semi-implicit hall-mhd solver using whistler wave preconditioning,” *Computer Physics Communications*, vol. 178, no. 8, pp. 553–557, 2008.
- [10] G. Toth, Y. Ma, and T. I. Gombosi, “Hall magnetohydrodynamics on block-adaptive grids,” *J. Comput. Phys.*, vol. 227, pp. 6967–6984, JUL 1 2008.
- [11] H. Lütjens and J.-F. Luciani, “Xtor-2f: a fully implicit newton–krylov solver applied to nonlinear 3d extended mhd in tokamaks,” *Journal of Computational Physics*, vol. 229, no. 21, pp. 8130–8143, 2010.
- [12] F. Laakmann, K. Hu, and P. E. Farrell, “Structure-preserving and helicity-conserving finite element approximations and preconditioning for the hall mhd equations,” *Journal of Computational Physics*, vol. 492, p. 112410, 2023.
- [13] J. Birn, J. F. Drake, M. A. Shay, B. N. Rogers, R. E. Denton, M. Hesse, M. M. Kuznetsova, Z. W. Ma, A. Bhattacharjee, A. Otto, and P. L. Pritchett, “Geospace Environment Modeling (GEM) magnetic reconnection challenge,” *J. Geophys. Res.*, vol. 106, no. A3, pp. 3715–3719, 2001.
- [14] X. Zhao, Y. Yang, and C. E. Seyler, “A positivity-preserving semi-implicit discontinuous galerkin scheme for solving extended magnetohydrodynamics equations,” *Journal of Computational Physics*, vol. 278, pp. 400–415, 2014.
- [15] C. Thoma, D. R. Welch, and D. V. Rose, “Implicit highly-coupled single-ion hall-mhd formulation for hybrid particle-in-cell codes,” *Computer Physics Communications*, vol. 261, p. 107823, 2021.
- [16] E. G. Phillips, J. N. Shadid, E. C. Cyr, and S. T. Miller, “Enabling scalable multifluid plasma simulations through block preconditioning,” *Numerical Methods for Flows: FEF 2017 Selected Contributions*, pp. 231–244, 2020.
- [17] M. M. Crockatt, S. Mabuza, J. N. Shadid, S. Conde, T. M. Smith, and R. P. Pawlowski, “An implicit monolithic afc stabilization method for the cg finite element discretization of the fully-ionized ideal multifluid electromagnetic plasma system,” *Journal of Computational Physics*, vol. 464, p. 111228, 2022.
- [18] L. Chacón, “An optimal, parallel, fully implicit Newton-Krylov solver for three-dimensional visco-resistive magnetohydrodynamics,” *Phys. Plasmas*, vol. 15, p. 056103, 2008.
- [19] Y. Saad, *Iterative Methods for Sparse Linear Systems*. Boston: PWS Publishing Company, 1996.
- [20] T. F. Chan and K. R. Jackson, “Nonlinearly preconditioned Krylov subspace methods for discrete Newton algorithms,” *SIAM J. Sci. Stat. Comput.*, vol. 5, pp. 533–542, 1984.
- [21] P. N. Brown and Y. Saad, “Hybrid Krylov methods for nonlinear systems of equations,” *SIAM J. Sci. Stat. Comput.*, vol. 11, pp. 450–481, 1990.

- [22] Y. Saad and M. Schultz, “GMRES: A generalized minimal residual algorithm for solving non-symmetric linear systems,” *SIAM J. Sci. Stat. Comput.*, vol. 7, pp. 856–869, 1986.
- [23] Y. Saad, “A flexible inner-outer preconditioned GMRES algorithm,” *SIAM J. Sci. Comput.*, vol. 14, no. 2, pp. 461–469, 1992.
- [24] F. Hülsemann, M. Kowarschik, M. Mohr, and U. Råde, “Parallel geometric multigrid,” in *Numerical Solution of Partial Differential Equations on Parallel Computers*, pp. 165–208, Springer, 2006.
- [25] D. A. May, P. Sanan, K. Rupp, M. G. Knepley, and B. F. Smith, “Extreme-scale multigrid components within petsc,” in *Proceedings of the Platform for Advanced Scientific Computing Conference*, pp. 1–12, 2016.
- [26] S. I. Braginskii, “Transport processes in a plasma,” in *Reviews of Plasma Physics* (M. A. Leontovich, ed.), vol. 1, pp. 205–311, New York: Consultants Bureau, 1965.
- [27] D. Biskamp, *Magnetic Reconnection in Plasmas*. Cambridge, UK: Cambridge University Press, 2000.
- [28] A. S. Kingsep, K. V. Chukbar, and V. V. Yan’kov, *Reviews of Plasma Physics*, vol. 16, pp. 243–288. New York: Consultants Bureau, 1990.
- [29] D. G. Swanson, *Plasma waves*. IOP Publishing, 2nd ed., 2003.
- [30] L. Chacón, “A non-staggered, conservative, $\nabla \cdot \mathbf{B} = \mathbf{0}$, finite-volume scheme for 3D implicit extended magnetohydrodynamics in curvilinear geometries,” *Comput. Phys. Commun.*, vol. 163, pp. 143–171, 2004.
- [31] G. D. Byrne and A. C. Hindmarsh, “A polyalgorithm for the numerical solution of ordinary differential equations,” *ACM Transactions on Mathematical Software*, vol. 1, no. 1, pp. 71–96, 1975.
- [32] D. A. Knoll and D. E. Keyes, “Jacobian-free Newton-Krylov methods: a survey of approaches and applications,” *J. Comput. Phys.*, vol. 193, no. 2, pp. 357 – 97, 2004.
- [33] P. Wesseling, *An Introduction to Multigrid Methods*. Chichester: John Wiley & Sons, 1992.
- [34] L. Chacón, D. A. Knoll, and J. M. Finn, “Implicit, nonlinear reduced resistive MHD nonlinear solver,” *J. Comput. Phys.*, vol. 178, no. 1, pp. 15–36, 2002.
- [35] H. C. Elman, V. E. Howle, J. N. Shadid, and R. S. Tuminaro, “A parallel block multi-level preconditioner for the 3D incompressible Navier-Stokes equations,” *J. Comput. Phys.*, vol. 187, no. 2, pp. 504 – 23, 2003.
- [36] H. Elman, V. E. Howle, J. Shadid, R. Shuttleworth, and R. Tuminaro, “Block preconditioners based on approximate commutators,” *SIAM Journal on Scientific Computing*, vol. 27, no. 5, pp. 1651–1668, 2006.
- [37] H. Elman, V. E. Howle, J. Shadid, R. Shuttleworth, and R. Tuminaro, “A taxonomy and comparison of parallel block multi-level preconditioners for the incompressible navier–stokes equations,” *Journal of Computational Physics*, vol. 227, no. 3, pp. 1790–1808, 2008.
- [38] E. C. Cyr, J. N. Shadid, and R. S. Tuminaro, “Stabilization and scalable block preconditioning for the navier–stokes equations,” *Journal of Computational Physics*, vol. 231, no. 2, pp. 345–363, 2012.

- [39] E. C. Cyr, J. N. Shadid, R. S. Tuminaro, R. P. Pawlowski, and L. Chacón, “A new approximate block factorization preconditioner for two-dimensional incompressible (reduced) resistive mhd,” *SIAM Journal on Scientific Computing*, vol. 35, no. 3, pp. B701–B730, 2013.
- [40] E. G. Phillips, J. N. Shadid, E. C. Cyr, H. C. Elman, and R. P. Pawlowski, “Block preconditioners for stable mixed nodal and edge finite element representations of incompressible resistive mhd,” *SIAM Journal on Scientific Computing*, vol. 38, no. 6, pp. B1009–B1031, 2016.
- [41] J. Bonilla, J. Shadid, X.-Z. Tang, M. Crockatt, P. Ohm, E. Phillips, R. Pawlowski, S. Conde, and O. Beznosov, “On a fully-implicit vms-stabilized fe formulation for low mach number compressible resistive mhd with application to mcf,” *Computer Methods in Applied Mechanics and Engineering*, vol. 417, p. 116359, 2023.
- [42] E. J. Caramana, “Derivation of implicit difference schemes by the method of differential approximation,” *J. Comput. Phys.*, vol. 96, no. 2, pp. 484–493, 1991.
- [43] D. S. Harned and W. Kerner, “Semi-implicit method for three-dimensional compressible magnetohydrodynamic simulation,” *J. Comput. Phys.*, vol. 60, pp. 62–75, 1985.
- [44] D. S. Harned and D. D. Schnack, “Semi-implicit method for long time scale magnetohydrodynamic computations in three dimensions,” *J. Comput. Phys.*, vol. 65, pp. 57–70, 1986.
- [45] R. Dembo, S. Eisenstat, and R. Steihaug, “Inexact Newton methods,” *J. Numer. Anal.*, vol. 19, p. 400, 1982.
- [46] W. L. Briggs, *A Multigrid Tutorial*. Philadelphia, PA: SIAM, 1987.
- [47] V. S. Lukin, A. H. Glasser, W. Lowrie, and E. T. Meier, “Overview of hifi-implicit spectral element code framework for multi-fluid plasma applications,” *arXiv preprint arXiv:1608.06030*, 2016.
- [48] L. Chacón and G. Lapenta, “A fully implicit, nonlinear adaptive grid strategy,” *J. Comput. Phys.*, vol. 212, no. 2, p. 703, 2006.
- [49] B. Srinivasan and U. Shumlak, “Analytical and computational study of the ideal full two-fluid plasma model and asymptotic approximations for hall-magnetohydrodynamics,” *Physics of Plasmas*, vol. 18, no. 9, 2011.

Appendix A. Analysis of the smoothing property of the damped-Jacobi iteration for the linearized EMHD system

We specialize the linearized EMHD system in Eq. 21 for a homogeneous uniform plasma in a periodic domain with a constant magnetic field (and therefore no background current) and no electron flow or electron inertia. The corresponding linear system reads:

$$\begin{aligned} \delta \mathbf{A} + \Delta t \theta d_i (v_A \delta \mathbf{j} \times \mathbf{B}_0 - d_i v_e \nabla^2 \delta \mathbf{j}) &= \mathbf{0}, \\ \delta \mathbf{j} - \nabla \times \nabla \times \delta \mathbf{A} &= \mathbf{0}. \end{aligned} \tag{A.1}$$

We have explicitly added the Alfvén speed v_A to keep track of dimensionless numbers later. In matrix form, the system can be written as:

$$\begin{bmatrix} \mathbb{I} & \Delta t \theta d_i [v_A \mathbb{I} \times \mathbf{B}_0 - d_i v_e \nabla^2] \\ -\nabla \times \nabla \times & \mathbb{I} \end{bmatrix} \begin{bmatrix} \delta \mathbf{A} \\ \delta \mathbf{j} \end{bmatrix} = \begin{bmatrix} \mathbf{0} \\ \mathbf{0} \end{bmatrix}.$$

Calling $\vec{\xi} = (\delta\mathbf{A}, \delta\mathbf{j})^T$, we can write the damped Jacobi iteration as:

$$\vec{\xi}^{l+1} = (\mathbb{I} - \sigma D^{-1}A)\vec{\xi}^l, \quad (\text{A.2})$$

where A is the matrix above, D is its diagonal (element- or block-wise), and $\sigma \in (0, 1]$ is the damping parameter. For simplicity, we restrict the analysis below to 2D and consider a uniform mesh with $\Delta x = \Delta y = \Delta$ as a sufficiently representative case for the challenges at hand.

In this study, we consider the block diagonal matrix formed by the diagonal coefficients of all vector components at a given cell, with one important approximation: $-\nabla \times \nabla \times \approx \nabla^2$ in the current density equation. As we shall see, this approximation delivers a convergent Jacobi iteration while avoiding the MG difficulties originating in the $\nabla \times \nabla \times$ term without changing the solution to the linear system upon convergence. There results:

$$D = \begin{bmatrix} \mathbb{I} & \Delta t \theta d_i [v_A \mathbb{I} \times \mathbf{B}_0 + d_i v_e \frac{4}{\Delta^2} \mathbb{I}] \\ -\frac{4}{\Delta^2} \mathbb{I} & \mathbb{I} \end{bmatrix} = \begin{bmatrix} \mathbb{I} & U \\ L & \mathbb{I} \end{bmatrix}, \quad (\text{A.3})$$

where:

$$U = \Delta t \theta d_i \left[v_A \mathbb{I} \times \mathbf{B}_0 + d_i v_e \frac{4}{\Delta^2} \mathbb{I} \right], \quad L = -\frac{4}{\Delta^2} \mathbb{I}.$$

The inverse of the diagonal matrix D is exactly given by:

$$D^{-1} = \begin{bmatrix} \mathbb{I} & -U \\ 0 & \mathbb{I} \end{bmatrix} \begin{bmatrix} \mathbb{I} & 0 \\ 0 & P^{-1} \end{bmatrix} \begin{bmatrix} \mathbb{I} & 0 \\ -L & \mathbb{I} \end{bmatrix} = \begin{bmatrix} \mathbb{I} + UP^{-1}L & -UP^{-1} \\ -P^{-1}L & P^{-1} \end{bmatrix} = \begin{bmatrix} P^{-1} & -\frac{\Delta^2}{4} [\mathbb{I} - P^{-1}] \\ \frac{4}{\Delta^2} P^{-1} & P^{-1} \end{bmatrix},$$

where:

$$P = \mathbb{I} - LU = \alpha \mathbb{I} + \beta (\mathbb{I} \times \mathbf{B}_0),$$

with:

$$\alpha = 1 + \frac{4v_e d_i}{v_A \Delta^2} \beta; \quad \beta = \frac{4\Delta t \theta v_A d_i}{\Delta^2}. \quad (\text{A.4})$$

Here, $\beta \gg 1$ is the whistler CFL number (which ensures we are in the stiff hyperbolic limit). The ratio α/β determines the dissipation regime. If we choose v_e such that dissipation is provided at the grid scale, and have $v_e \sim v_A \Delta^2/d_i$ and therefore $\alpha \sim \beta \gg 1$. Weak and strong hyperresistivity regimes are then defined by $\alpha \ll \beta$ and $\alpha \gg \beta$, respectively. The matrix P has an analytical inverse, given by:

$$P^{-1} = \frac{\alpha \mathbb{I} - \beta (\mathbb{I} \times \mathbf{B}_0) + \frac{\beta^2}{\alpha} (\mathbb{I} \cdot \mathbf{B}_0) \mathbf{B}_0}{\alpha^2 + \beta^2}.$$

To study the convergence properties of the Jacobi iteration, we perform a Von-Neumann analysis with the ansatz:

$$\vec{\xi}^l = \lambda^l e^{i\mathbf{k} \cdot \mathbf{x}} \vec{\xi}^0,$$

where λ is the Jacobi iteration amplification factor. Stability of the iteration demands $|\lambda| \leq 1$. The smoothing property requires $|\lambda| < 1$ for the high-wavenumber modes in the system. With this ansatz, we can diagonalize our differential operators as:

$$\begin{aligned} \nabla^2 &\rightarrow -\left(k_x^2 \text{sinc}^2\left(\frac{k_x \Delta}{2}\right) + k_y^2 \text{sinc}^2\left(\frac{k_y \Delta}{2}\right) \right) = -\kappa_L^2, \\ \nabla &\rightarrow i(k_x \text{sinc}(k_x \Delta), k_y \text{sinc}(k_y \Delta)) = i\kappa_G, \\ \nabla \times \nabla \times &\rightarrow -\kappa_G \times \kappa_G \times, \end{aligned}$$

where $\text{sinc}(x) = \sin(x)/x$. The JB iteration in Eq. A.2 then yields the equation for the amplification factor:

$$(1 - \lambda) \begin{bmatrix} \mathbb{I} & 0 \\ 0 & \mathbb{I} \end{bmatrix} = \sigma \begin{bmatrix} \mathbb{I} + K [P^{-1} - \mathbb{I}] & \frac{\Delta^2}{4} \gamma P^{-1} \\ \frac{4\sigma}{\Delta^2} K P^{-1} & \mathbb{I} + \gamma P^{-1} \end{bmatrix}, \quad (\text{A.5})$$

where:

$$\gamma = \frac{d_i v_e}{v_A} \beta \left(\kappa_L^2 - \frac{4}{\Delta^2} \right) = (\alpha - 1) (\hat{\kappa}_L^2 - 1),$$

and:

$$K = [\mathbb{I} + \hat{\mathbf{k}}_G \times \hat{\mathbf{k}}_G \times \mathbb{I}],$$

with:

$$\hat{\kappa}_L^2 = \frac{\Delta^2 \kappa_L^2}{4} = \left(\frac{\Delta^2 k_x^2}{4} \text{sinc}^2 \left(\frac{k_x \Delta}{2} \right) + \frac{\Delta^2 k_y^2}{4} \text{sinc}^2 \left(\frac{k_y \Delta}{2} \right) \right) = \sin^2 \left(\frac{k_x \Delta}{2} \right) + \sin^2 \left(\frac{k_y \Delta}{2} \right) \in (0, 2] \quad (\text{A.6})$$

$$\hat{\mathbf{k}}_G = \frac{\Delta \kappa_G}{2} = \frac{1}{2} (k_x \Delta \text{sinc}(k_x \Delta), k_y \Delta \text{sinc}(k_y \Delta)) = (\sin(k_x \Delta), \sin(k_y \Delta)).$$

Therefore, Eq. A.5 yields:

$$\begin{bmatrix} (\lambda - 1 + \sigma) \mathbb{I} + \sigma K [P^{-1} - \mathbb{I}] & \frac{\sigma \Delta^2}{4} \gamma P^{-1} \\ \frac{4\sigma}{\Delta^2} K P^{-1} & (\lambda - 1 + \sigma) \mathbb{I} + \sigma \gamma P^{-1} \end{bmatrix} = 0. \quad (\text{A.7})$$

Equation A.7 is a 2×2 block matrix with commuting blocks. The solution for λ is given by the determinant of the matrix being zero. The determinant can be found as (proof via a Schur factorization):

$$\det \left[(\lambda^*)^2 P + \lambda^* \sigma [\gamma \mathbb{I} + K(\mathbb{I} - P)] - \sigma^2 \gamma K \right] = 0.$$

Restricting the analysis to the stiff hyperbolic limit [$\alpha \gg 1$, which implies $(\mathbb{I} - P) \approx -P$ and $\gamma \approx \alpha (\hat{\kappa}_L^2 - 1)$], we find:

$$\det \left[(\lambda^*)^2 \frac{P}{\alpha} + \lambda^* \sigma \left[(\hat{\kappa}_L^2 - 1) \mathbb{I} - K \frac{P}{\alpha} \right] - \sigma^2 (\hat{\kappa}_L^2 - 1) K \right] = 0. \quad (\text{A.8})$$

Here:

$$\frac{P}{\alpha} = \mathbb{I} + \frac{\beta}{\alpha} (\mathbb{I} \times \mathbf{B}_0),$$

and:

$$\frac{\beta}{\alpha} \approx \frac{v_A \Delta^2}{4 v_e d_i}.$$

Equation A.8 will be the starting point to analyze three dissipation regimes of interest, all of them in the strongly hyperbolic limit ($\beta \gg 1$): the strong hyperresistivity regime, the weak one, and the balanced regime with hyperresistivity dissipation at the grid scale.

Strong hyperresistivity regime: $\beta \ll \alpha$. In this case, we have:

$$\left(\frac{P}{\alpha}\right)^{-1} = \alpha P^{-1} \approx \mathbb{I} - \frac{\beta}{\alpha}(\mathbb{I} \times \mathbf{B}_0).$$

There results:

$$\det \left[(\lambda^*)^2 \mathbb{I} + \lambda^* \sigma \left[(\hat{\kappa}_L^2 - 1) \left(\mathbb{I} - \frac{\beta}{\alpha}(\mathbb{I} \times \mathbf{B}_0) \right) - K \right] - \sigma^2 (\hat{\kappa}_L^2 - 1) K \left(\mathbb{I} - \frac{\beta}{\alpha}(\mathbb{I} \times \mathbf{B}_0) \right) \right] = 0.$$

Taking the $\beta/\alpha \rightarrow 0$ limit, we have:

$$\det \left[(\lambda^*)^2 \mathbb{I} + \lambda^* \sigma [(\hat{\kappa}_L^2 - 1) \mathbb{I} - K] - \sigma^2 (\hat{\kappa}_L^2 - 1) K \right] = 0.$$

This leads to a sixth-order characteristic polynomial, with six roots. In vector form:

$$[\lambda^* + \sigma (\hat{\kappa}_L^2 - 1)] [\xi \mathbf{A} - K \mathbf{A}] = 0, \quad (\text{A.9})$$

with $\xi = \frac{\lambda^*}{\sigma}$. This has the solution (with multiplicity three, applying to all vector components):

$$\boxed{\lambda_L = 1 - \sigma \hat{\kappa}_L^2}.$$

Taking components of the remainder of Eq. A.9, and noting that [assuming $B_0 = 1$ without loss of generality and defining $A_{\parallel} = \mathbf{A} \cdot \mathbf{B}_0$, $A_k = \hat{\kappa}_G \cdot \mathbf{A}$, $A_{\times, \parallel} = \mathbf{B}_0 \cdot (\hat{\kappa}_G \times \mathbf{A})$]:

$$\hat{\kappa}_G \cdot K \mathbf{A} = A_k ; \hat{\kappa}_G \times K \mathbf{A} = K (\hat{\kappa}_G \times \mathbf{A}) ; \mathbf{B}_0 \cdot K \mathbf{A} = (1 - \hat{\kappa}_G^2) A_{\parallel} + A_k \hat{\kappa}_{\parallel, G},$$

we find:

- $\mathbf{B}_0 \cdot [\dots] \Rightarrow \xi A_{\parallel} - (1 - \hat{\kappa}_G^2) A_{\parallel} + A_k \hat{\kappa}_{\parallel, G} = 0,$
- $\hat{\kappa}_G \cdot [\dots] \Rightarrow \xi A_k - A_k = 0 \Rightarrow \xi = 1 \Rightarrow \boxed{\lambda = 1},$
- $\mathbf{B}_0 \cdot [\hat{\kappa}_G \times [\dots]] \Rightarrow \xi A_{\times, \parallel} - (1 - \hat{\kappa}_G^2) A_{\times, \parallel} = 0 \Rightarrow \boxed{\lambda_G = 1 - \sigma \hat{\kappa}_G^2}.$

The first equation with $A_k = 0$ (from the second equation for $\lambda \neq 1$) also gives;

$$\boxed{\lambda_G = 1 - \sigma \hat{\kappa}_G^2}.$$

We have now found all six eigenvalues for the Jacobi amplification factor, and they are all stable ($|\lambda| \leq 1$). However, only λ_L allows for the smoothing property. In particular, from the definition of $\hat{\kappa}_L^2$ in Eq. A.6, for the Nyquist mode $k_x = k_x = \pi/\Delta$ we have $\hat{\kappa}_L^2 = 2$ and therefore $\lambda_L = 1 - 2\sigma$, which implies strong damping for a suitably chosen $\sigma \in (0, 1]$ (e.g., $\sigma = 0.7$) and therefore a robust smoothing property for error components at the grid scale. This is not the case for λ_G , since for the Nyquist mode $\hat{\kappa}_G^2 = 0$ and therefore $\lambda_G = 1$. This difference in smoothing behavior stems from the fact that $\hat{\kappa}_G^2$ originates in the central difference discretization of a gradient, whereas $\hat{\kappa}_L^2$ originates in the usual Laplacian discretization. That said, for the strong hyperresistivity regime, λ_L has multiplicity three and is affecting all vector components simultaneously, and is therefore providing strong smoothing to the whole system.

Weak hyperresistivity regime: $\alpha \ll \beta$. In this case, we have:

$$\left(\frac{P}{\alpha}\right)^{-1} = \alpha P^{-1} = \frac{\alpha^2/\beta^2 \mathbb{I} - \alpha/\beta (\mathbb{I} \times \mathbf{B}_0) + (\mathbb{I} \cdot \mathbf{B}_0) \mathbf{B}_0}{\alpha^2/\beta^2 + 1} \approx (\mathbb{I} \cdot \mathbf{B}_0) \mathbf{B}_0 - \frac{\alpha}{\beta} (\mathbb{I} \times \mathbf{B}_0).$$

Taking the $\alpha/\beta \rightarrow 0$ limit, there results:

$$\det \left[(\lambda^*)^2 \mathbb{I} + \lambda^* \sigma \left[(\hat{\kappa}_L^2 - 1) (\mathbb{I} \cdot \mathbf{B}_0) \mathbf{B}_0 - K \right] - \sigma^2 (\hat{\kappa}_L^2 - 1) K (\mathbb{I} \cdot \mathbf{B}_0) \mathbf{B}_0 \right] = 0.$$

In vector form, the determinant equation can be written as:

$$(\lambda^*)^2 \mathbf{A} + \lambda^* \sigma \left[(\hat{\kappa}_L^2 - 1) A_{\parallel} \mathbf{B}_0 - K \mathbf{A} \right] - \sigma^2 (\hat{\kappa}_L^2 - 1) A_{\parallel} K \mathbf{B}_0 = 0.$$

Taking components of this equation, we find:

- $\mathbf{B}_0 \cdot [\dots] \Rightarrow (\lambda^*)^2 A_{\parallel} + \lambda^* \sigma \left[(\hat{\kappa}_L^2 + \hat{\kappa}_G^2 - 2) A_{\parallel} - A_k \hat{\kappa}_{\parallel, G} \right] - \sigma^2 (\hat{\kappa}_L^2 - 1) (1 - \hat{\kappa}_{\perp, G}^2) A_{\parallel} = 0$, or:

$$\left(\left(\frac{\lambda^*}{\sigma} \right)^2 + \frac{\lambda^*}{\sigma} (\hat{\kappa}_L^2 + \hat{\kappa}_G^2 - 2) - (\hat{\kappa}_L^2 - 1) (1 - \hat{\kappa}_{\perp, G}^2) \right) A_{\parallel} - \frac{\lambda^*}{\sigma} \hat{\kappa}_{\parallel, G} A_k = 0.$$

- $\hat{\kappa}_G \cdot [\dots] \Rightarrow (\lambda^*)^2 A_k + \lambda^* \sigma \left[(\hat{\kappa}_L^2 - 1) A_{\parallel} \hat{\kappa}_{\parallel, G} - A_k \right] - \sigma^2 (\hat{\kappa}_L^2 - 1) A_{\parallel} \hat{\kappa}_{\parallel, G} = 0$ or:

$$(\lambda^* - \sigma) \left[\frac{\lambda^*}{\sigma} A_k + (\hat{\kappa}_L^2 - 1) \hat{\kappa}_{\parallel, G} A_{\parallel} \right] = 0 \Rightarrow \boxed{\lambda = 1}; \frac{\lambda^*}{\sigma} A_k + (\hat{\kappa}_L^2 - 1) \hat{\kappa}_{\parallel, G} A_{\parallel} = 0.$$

- $\mathbf{B}_0 \cdot [\hat{\kappa}_G \times [\dots]] \Rightarrow (\lambda^*)^2 A_{\times, \parallel} - \lambda^* \sigma (1 - \hat{\kappa}_G^2) A_{\times, \parallel} = 0 \Rightarrow \boxed{\lambda = 1 - \sigma}; \boxed{\lambda_G = 1 - \sigma \hat{\kappa}_G^2}.$

Solving the first two equations, we find (in terms of $\xi = \lambda^*/\sigma$):

$$\boxed{\lambda = 1 - \sigma}; \xi^2 + \xi (\hat{\kappa}_L^2 + \hat{\kappa}_G^2 - 2) + (\hat{\kappa}_L^2 - 1) (\hat{\kappa}_G^2 - 1) = 0,$$

gives:

$$\xi = 1 - \hat{\kappa}_L^2; \xi = 1 - \hat{\kappa}_G^2,$$

which finally results in:

$$\boxed{\lambda_L = 1 - \sigma \hat{\kappa}_L^2; \lambda_G = 1 - \sigma \hat{\kappa}_G^2}.$$

For this case, we find that the problematic amplification factor λ_G is present for all three components, but is always accompanied by a strongly damping one, either $(1 - \sigma)$ (for $A_{\times, \parallel}$) or λ_L (for A_{\parallel}, A_k), therefore resulting in effective smoothing even without hyperresistivity.

Grid-scale hyperresistivity regime: $\beta/\alpha = 1$. For this case, we have:

$$\det \left[(\lambda^*)^2 \mathbb{I} + \lambda^* \sigma \left[(\hat{\kappa}_L^2 - 1) \alpha P^{-1} - K \right] - \sigma^2 (\hat{\kappa}_L^2 - 1) K \alpha P^{-1} \right] = 0$$

with:

$$\alpha P^{-1} = \frac{\mathbb{I} - (\mathbb{I} \times \mathbf{B}_0) + (\mathbb{I} \cdot \mathbf{B}_0) \mathbf{B}_0}{2}.$$

This system can be expressed in vector form as:

$$(\lambda^*)^2 \mathbf{A} + \lambda^* \sigma \left[(\hat{\kappa}_L^2 - 1) (\alpha P^{-1}) \mathbf{A} - K \mathbf{A} \right] - \sigma^2 (\hat{\kappa}_L^2 - 1) K (\alpha P^{-1}) \mathbf{A} = 0,$$

with:

$$\alpha P^{-1} \mathbf{A} = \frac{\mathbf{A} - \mathbf{A} \times \mathbf{B}_0 + A_{\parallel} \mathbf{B}_0}{2}.$$

Taking components of this equation, noting that:

- $\hat{\mathbf{k}}_G \cdot (\alpha P^{-1})\mathbf{A} = \frac{A_k - A_{\times, \parallel} + A_{\parallel} \hat{\mathbf{k}}_{\parallel, G}}{2}$.
- $\mathbf{B}_0 \cdot (\hat{\mathbf{k}}_G \times (\alpha P^{-1})\mathbf{A}) = \frac{A_{\times, \parallel} - A_{\parallel} \hat{\mathbf{k}}_{\parallel, G} + A_k}{2}$.
- $\mathbf{B}_0 \cdot (\alpha P^{-1})\mathbf{A} = A_{\parallel}$.

we find:

- $\mathbf{B}_0 \cdot [\dots] \Rightarrow$

$$\left((\lambda^*)^2 + \lambda^* \sigma (\hat{\mathbf{k}}_G^2 + \hat{\mathbf{k}}_L^2 - 2) - \sigma^2 (\hat{\mathbf{k}}_L^2 - 1) (1 - \hat{\mathbf{k}}_G^2) \right) A_{\parallel} - \lambda^* \sigma A_k \hat{\mathbf{k}}_{\parallel, G} - \sigma^2 (\hat{\mathbf{k}}_L^2 - 1) \hat{\mathbf{k}}_{\parallel, G} \frac{A_k - A_{\times, \parallel} + A_{\parallel} \hat{\mathbf{k}}_{\parallel, G}}{2} = 0$$
, or:

$$\left(\left(\frac{\lambda^*}{\sigma} \right)^2 + \frac{\lambda^*}{\sigma} (\hat{\mathbf{k}}_G^2 + \hat{\mathbf{k}}_L^2 - 2) - (\hat{\mathbf{k}}_L^2 - 1) (1 - \hat{\mathbf{k}}_G^2) \right) A_{\parallel} - \frac{\lambda^*}{\sigma} A_k \hat{\mathbf{k}}_{\parallel, G} - (\hat{\mathbf{k}}_L^2 - 1) \hat{\mathbf{k}}_{\parallel, G} \frac{A_k - A_{\times, \parallel} + A_{\parallel} \hat{\mathbf{k}}_{\parallel, G}}{2} = 0$$

- $\hat{\mathbf{k}}_G \cdot [\dots] \Rightarrow \left((\lambda^*)^2 - \lambda^* \sigma \right) A_k + [\lambda^* \sigma - \sigma^2] (\hat{\mathbf{k}}_L^2 - 1) \frac{A_k - A_{\times, \parallel} + A_{\parallel} \hat{\mathbf{k}}_{\parallel, G}}{2} = 0$, or:

$$(\lambda^* - \sigma) \left[\frac{\lambda^*}{\sigma} A_k + (\hat{\mathbf{k}}_L^2 - 1) \frac{A_k - A_{\times, \parallel} + A_{\parallel} \hat{\mathbf{k}}_{\parallel, G}}{2} \right] = 0 \Rightarrow \boxed{\lambda = 1}; \frac{\lambda^*}{\sigma} A_k + (\hat{\mathbf{k}}_L^2 - 1) \frac{A_k - A_{\times, \parallel} + A_{\parallel} \hat{\mathbf{k}}_{\parallel, G}}{2} = 0.$$

- $\mathbf{B}_0 \cdot [\hat{\mathbf{k}}_G \times [\dots]] \Rightarrow$

$$(\lambda^*)^2 A_{\times, \parallel} + \lambda^* \sigma (\hat{\mathbf{k}}_L^2 - 1) \frac{A_{\times, \parallel} - A_{\parallel} \hat{\mathbf{k}}_{\parallel, G} + A_k}{2} - \lambda^* \sigma (1 - \hat{\mathbf{k}}_G^2) A_{\times, \parallel} - \sigma^2 (\hat{\mathbf{k}}_L^2 - 1) (1 - \hat{\mathbf{k}}_G^2) \frac{A_{\times, \parallel} - A_{\parallel} \hat{\mathbf{k}}_{\parallel, G} + A_k}{2} = 0,$$

or:

$$[\lambda^* - \sigma (1 - \hat{\mathbf{k}}_G^2)] \left[\lambda^* A_{\times, \parallel} + \sigma (\hat{\mathbf{k}}_L^2 - 1) \frac{A_{\times, \parallel} - A_{\parallel} \hat{\mathbf{k}}_{\parallel, G} + A_k}{2} \right] = 0,$$

and therefore:

$$\boxed{\lambda_G = 1 - \sigma \hat{\mathbf{k}}_G^2}; \frac{\lambda^*}{\sigma} A_{\times, \parallel} + (\hat{\mathbf{k}}_L^2 - 1) \frac{A_{\times, \parallel} - A_{\parallel} \hat{\mathbf{k}}_{\parallel, G} + A_k}{2} = 0.$$

Solving the first two equations, we find:

$$\left(\frac{\lambda^*}{\sigma} \right)^2 + \frac{\lambda^*}{\sigma} (\hat{\mathbf{k}}_G^2 + \hat{\mathbf{k}}_L^2 - 2) + (\hat{\mathbf{k}}_L^2 - 1) (\hat{\mathbf{k}}_G^2 - 1) = 0,$$

or:

$$\boxed{\lambda_L = 1 - \sigma \hat{\mathbf{k}}_L^2; \lambda_G = 1 - \sigma \hat{\mathbf{k}}_G^2}.$$

Else, $A_{\parallel} = 0$, and from the last two equations we find:

$$\begin{aligned} \lambda^* A_{\times, \parallel} + \frac{\sigma (\hat{\mathbf{k}}_L^2 - 1)}{2} (A_{\times, \parallel} + A_k) &= 0, \\ \lambda^* A_k + \frac{\sigma (\hat{\mathbf{k}}_L^2 - 1)}{2} (A_k - A_{\times, \parallel}) &= 0. \end{aligned}$$

Solving, we find two complex conjugate roots:

$$\boxed{\lambda = 1 - \sigma \left(1 + \frac{\hat{\mathbf{k}}_L^2 - 1}{2} \right) \pm i \sigma \frac{|\hat{\mathbf{k}}_L^2 - 1|}{2}}.$$

Recall that $|\hat{\kappa}_L^2 - 1| \in [0, 1]$, that for stability of the Jacobi iteration we need $|\lambda| \leq 1$, and for the smoothing property we need the strict inequality for the Nyquist mode. Computing $|\lambda|$, we find:

$$|\lambda|^2 = (1 - \sigma)^2 - (1 - \sigma)\sigma(\hat{\kappa}_L^2 - 1) + \sigma^2 \frac{(\hat{\kappa}_L^2 - 1)^2}{2}, \quad (\text{A.10})$$

and therefore it follows that:

$$|\lambda| < 1 \Rightarrow \sigma < \frac{2(1 + \hat{\kappa}_L^2)}{1 + \hat{\kappa}_L^4}.$$

This condition is always satisfied, as the right hand side is always greater than unity for $\hat{\kappa}_L^2 \in [0, 2]$, and $\sigma \in (0, 1]$. Therefore, these roots are stable and strongly damping for the Nyquist mode $\hat{\kappa}_L^2 = 2$. This can be shown by introducing $\hat{\kappa}_L^2$ into Eq. A.10, to find:

$$|\lambda|^2 = 1 - 3\sigma + \frac{5}{2}\sigma^2,$$

which is always less than unity for $\sigma \in (0, 1]$, and results in very strong damping of the Nyquist mode for a suitably chosen damping parameter: $|\lambda|^2 = 0.1$ for $\sigma = 0.6$.

As in previous cases, we find the problematic amplification factor λ_G is present for all vector components, but always accompanied by a robustly smoothing one: λ_L for A_{\parallel} and two robustly smoothing complex conjugate amplification factors for $A_{\times, \parallel}$ and A_k . These ensure the smoothing property of the Jacobi iteration for the whole system.